Supplementary Information for

Polymorph-Triggered Multiple Responses in Dynamic Molecular Crystals of Barbituric Acid Derivatives

Ya-Bing Sun,[a] Jiang-Tao Liu,[a] Hui-Yao Lin,*[a] Chen-Chen Zhang,[a] Da-Hui Qu,[a] and Fei Tong*[a]

[a] Key Laboratory for Advanced Materials and Joint International Research Laboratory of Precision Chemistry and Molecular Engineering, Feringa Nobel Prize Scientist Joint Research Center, Frontiers Science Center for Materiobiology and Dynamic Chemistry, Institute of Fine Chemicals, School of Chemistry and Molecular Engineering, East China University of Science and Technology, Meilong Road 130, Shanghai 200237, China.

*E-mail address: huiyao_lin@ecust.edu.cn; feitong@ecust.edu.cn

Experimental Section

High-Resolution Electron Impact Mass Spectroscopy (HR-EI-MS) Measurements: All the samples were first dried in an oven at 45°C for 12 hours before measurements. HR EI-MS spectra were measured by using the GCT Premier TOF mass spectrometer (Waters Corporation, USA).

Single Crystal Preparation of Form A: First, dissolve about 7 mg of the sample in 1 mL of THF solution, filter it into an open-mouth glass bottle with a filter head, and then put it into a large glass bottle containing water seal the large beaker and wrap it with aluminum foil, and leave it for a certain period of time to carry out gas-liquid exchange between the two solvents and finally make the solution reach a state of supersaturation and precipitate large single crystals for Single crystal analysis.

Single Crystal Preparation of Form B: Firstly, about 6 mg of the sample was dissolved in 1 mL of THF solution and filtered through a filter head into an open 1ml glass bottle, then into a 20 mL glass bottle containing 5 mL of n-hexane, which was sealed and wrapped in aluminum foil and left to stand for a day, during which the two solvents were subjected to a gas-liquid exchange, which ultimately led to the solution reaching a state of supersaturation, precipitating large single crystals for single crystal analysis.

Single Crystal Preparation of Form C: Firstly, about 6 mg of the sample was dissolved in 1 mL of THF solution and filtered through a filter head into an open 1ml glass bottle, then into a 20 mL glass bottle containing 5 mL of n-hexane, which was sealed and wrapped in aluminum foil and left to stand for seven days, during which the two solvents were subjected to a gas-liquid exchange, which ultimately led to the solution reaching a state of supersaturation, precipitating large single crystals for single crystal analysis.

Single Crystal Preparation of Form D: Firstly, the sample was dissolved in 0.5 mL of DMF to prepare a saturated solution, which was then filtered. A 0.5 mL aliquot of the filtrate was placed in a 1 mL vial. This vial was then placed uncapped inside a 20 mL sealed container holding 5 mL of n-hexane. The entire setup was wrapped in aluminum foil to exclude light and allowed to stand at room temperature for 3-5 days, precipitating large single crystals for single crystal analysis.

Irradiation Experiments: For irradiated samples for routine NRI and spectroscopic measurements, the LED lamp (PLS-LED 100CLED, Beijing Perfect Light Technology Co. Ltd.) was placed with the head facing upwards and a surface dish was placed on top of the head of the lamp; the sample was placed horizontally on the

surface dish. For samples irradiated by microscope lamps, the distance between the lens and the sample depended on each lens (usually a few millimeters).

TGA & DSC measurement: The thermal stability was measured by thermal gravimetric analysis (TGA) under nitrogen and each sample was heated from room temperature to 800°C (SHIMADZU TGA-50, heating rate = 20°C/min). The melting point (Tm) was recorded by differential scanning calorimetry (DSC) under the nitrogen (SHIMADZU DSC-60Plus, heating rate = 10°C/min).

Thermal Heating Incorporated with Optical Microscope Characterization: An artificial-manufactured microscope thermal plate with the temperature console WT4000H (Wei-Tu Co., Ltd, Shanghai, China) was used to heat samples and sustain ambient temperature during the characterization. The thermal plate is controlled by software, and the heating rate is about 20℃/min before the temperature reaches the desired values.

Fourier Transform Infrared (FT-IR) Spectral Measurements: Samples of Form A, Form A-H, Form A-H-W, Form B, and Form B-W were placed on the sample stage for measurement using a Thermo Fisher Scientific Nicolet iS50R FT-IR Spectrometer. A background scan was performed prior to each sample measurement.

PXRD Measurements: All Forms were sent directly to the sample for detection. All PXRD data were collected at room temperature on an X-ray diffractometer (Rigaku, 18 kW/D/Max2550VB/PC, CuKα radiation, λ = 1.5418 Å, 40 kV/100 mA power). Samples were measured in the Prague-Brentano geometry. The sample holder was fixed horizontally and the detector (evanescent slit = 1.00 mm, no monochromator) was rotated on the sample with a step size = 0.02º.

Fluorescence Measurements: Steady-state fluorescence spectra were acquired using an FLS 1000 fluorescence spectrometer (Edinburgh Instruments, UK). Solid powder samples were evenly loaded into a quartz sample holder for spectral collection.

Measurement of quantum yield: Quantum yields were measured by using an integrating sphere on a HAMAMATSU Quantaurus QY C11347-11.

Variable-Temperature Powder X-ray Diffraction (VT-PXRD): VT-PXRD patterns were recorded on an Empyrean X-ray diffractometer (Malvern Panalytical, the Netherlands).

Packing Index: The packing index was calculated using the PLATON software (Spek, 2009) based on SCXRD data.

Independent gradient model based on Hirshfeld partition (IGMH) has been calculated at the functional B3LYP-D3BJ/6-311g(d,p) and m062x-D3/6-311+g(d,p) set on

crystal structures. Interaction energies were investigated by using sobEDAw, a novel energy decomposition method based on density functional theory (DFT), including dispersion corrections at the B3LYP-D3BJ/6-311g(d,p) level.[1–3]

Supplementary Movies

Movie S1: The transformation process of Form B into Form C upon heating, accompanied by a change in crystal color. The video was captured in a melting point apparatus while the real-time temperature is shown in the top-right corner. Scale bar: 200 μm.

Movie S2: Form B exhibits thermomechanical response behavior upon heating. Scale bar: 100 μm.

Movie S3: Form A exhibits a reversible photochromic process upon light or heating. Scale bar: 100 μm.

Single Crystal Information of Forms A-D crystal structure:

Table S1. Crystal data and structure refinement for Form A (CCDC number: 2518956).

Identification code	Form A	
Empirical formula	$C_{17}H_{12}N_2O_3 \cdot H_2O$	
Formula weight	310.30	
Temperature	179.00 K	
Wavelength	1.34139 Å	
Crystal system	Monoclinic	
Space group	$P2_1/n$	
Unit cell dimensions	a = 6.9648(5) Å	α = 90°
	b = 15.6277(11) Å	β = 104.605(3)°
	c = 13.0339(10) Å	γ = 90°
Volume	1372.82(17) $Å^3$	
Z	4	
Density (calculated)	1.501 Mg/m^3	
Absorption coefficient	0.575 mm^{-1}	
F(000)	648	
Crystal size	0.17 x 0.17 x 0.05 mm^3	
Theta range for data collection	3.918° to 55.149°	
Index ranges	-8<=h<=8, 0<=k<=18, 0<=l<=15	
Reflections collected	2592	
Independent reflections	2592 [R_{int} = ?， R_{sigma} = 0.0379]	
Completeness to theta = 53.594°	99.1 %	
Absorption correction	Semi-empirical from equivalents	
Max. and min. transmission	0.7508 and 0.5682	
Refinement method	Full-matrix least-squares on F^2	
Data / restraints / parameters	2592 / 0 / 221	
Goodness-of-fit on F^2	1.552	
Final R indices [I>2sigma(I)]	R_1 = 0.0921, wR_2 = 0.3124	
R indices (all data)	R_1 = 0.0988, wR_2 = 0.3294	
Extinction coefficient	0.028(9)	
Largest diff. peak and hole	0.506 and -0.399 e.$Å^{-3}$	

Table S2. Crystal data and structure refinement for Form B (CCDC number: 2518957).

Identification code	Form B	
Empirical formula	$C_{17}H_{12}N_2O_3$	
Formula weight	292.29	
Temperature	170.00 K	
Wavelength	1.54178Å	
Crystal system	orthorhombic	
Space group	$P2_12_12_1$	
Unit cell dimensions	a = 4.8581(2)Å	α = 90°
	b = 12.0824(4) Å	β = 90°
	c = 31.0459(13) Å	γ = 90°
Volume	1822.32(12) $Å^3$	
Z	4	
Density (calculated)	1.065 Mg/m^3	
Absorption coefficient	0.613 mm^{-1}	
F(000)	608	
Crystal size	0.19 × 0.018 × 0.008 mm^3	
Theta range for data collection	5.694° to 138.322°	
Index ranges	$-5 \leq h \leq 5$, $-14 \leq k \leq 14$, $-37 \leq l \leq 37$	
Reflections collected	26027	
Independent reflections	3370[R_{int} = 0.0812]	
Completeness to theta = 69.2°	99.1 %	
Absorption correction	Multi-scan (SADABS2016/2)	
Max. and min. transmission	0.604 and 0.753	
Refinement method	Full-matrix least-squares on F^2	
Data / restraints / parameters	3370 / 0 / 201	
Goodness-of-fit on F^2	1.06	
Final R indices [I>2sigma(I)]	R_1 = 0.0736, wR_2 = 0.2200	
R indices (all data)	R_1 = 0.0835, wR_2 = 0.2317	
Extinction coefficient	0.36(18)	
Largest diff. peak and hole	0.24 and -0.27.$Å^{-3}$	

Table S3. Crystal data and structure refinement for Form C (CCDC number: 2518958).

Identification code	Form C	
Empirical formula	$C_{17}H_{12}N_2O_3$	
Formula weight	292.29	
Temperature	150 K	
Wavelength	1.54178 Å	
Crystal system	Monoclinic	
Space group	$P2_1$	
Unit cell dimensions	a = 4.6351 (3) Å	α = 90°
	b = 11.8308 (7) Å	β = 92.295 (4)°
	c = 12.3552 (8) Å	γ = 90°
Volume	676.98 (7) $Å^3$	
Z	2	
Density (calculated)	1.434 Mg/m^3	
Absorption coefficient	0.83 mm^{-1}	
F(000)	304	
Crystal size	0.06 × 0.04 × 0.01 mm	
Theta range for data collection	3.6° to 75.0°	
Reflections collected	1443	
Independent reflections	1443 [R_{int} = 0.082]	
Refinement method	Full-matrix least-squares on F^2	
Data / restraints / parameters	1443 / 1 / 207	
Goodness-of-fit on F^2	1.10	
Final R indices [I>2sigma(I)]	R_1 = 0.085, wR_2 = 0.238	
Absolute structure parameter	0.0 (8)	
Largest diff. peak and hole	0.29 and -0.36 e $Å^{-3}$	

Table S4. Crystal data and structure refinement for Form D (CCDC number: 2518959).

Identification code	Form D	
Empirical formula	$C_{17}H_{12}N_2O_3$	
Formula weight	292.29	
Temperature	170.00 K	
Wavelength	1.34139 Å	
Crystal system	Orthorhombic	
Space group	Pbca	
Unit cell dimensions	a = 14.3120(10) Å	α = 90°
	b = 7.0353(5) Å	β = 90°
	c = 27.0739(17) Å	γ = 90°
Volume	2726.0(3) $Å^3$	
Z	8	
Density (calculated)	1.424 Mg/m^3	
Absorption coefficient	0.522 mm^{-1}	
F(000)	1216	
Crystal size	0.17 x 0.17 x 0.05 mm^3	
Theta range for data collection	3.910 to 55.074°	
Index ranges	-17<=h<=17, -8<=k<=8, -32<=l<=32	
Reflections collected	22420	
Independent reflections	2597 [R_{int} = 0.1116]	
Completeness to theta = 53.594°	99.6 %	
Absorption correction	Semi-empirical from equivalents	
Max. and min. transmission	0.7508 and 0.5375	
Refinement method	Full-matrix least-squares on F^2	
Data / restraints / parameters	2597 / 0 / 208	
Goodness-of-fit on F^2	1.039	
Final R indices [I>2sigma(I)]	R_1 = 0.0633, wR_2 = 0.1595	
R indices (all data)	R_1 = 0.0958, wR_2 = 0.1849	
Extinction coefficient	0.0019(6)	
Largest diff. peak and hole	0.231 and -0.258 e.$Å^{-3}$	

Compound Synthesis

Synthesis of (*E*)-3-(naphthalen-1-yl)acrylaldehyde **(*E*)-NAA**:

Acrolein diethyl acetal (3.900 g, 0.03 mol), nBu_4NOAc (6.040 g, 0.020 mol), K_2CO_3 (2.070 g, 0.015 mol), KCl (0.745 g, 0.010 mol), and $Pd(OAc)_2$ (0.068 g, 0.300 mmol) were added into a stirred solution of 1-bromonaphthalene (2.070 g, 0.01 mol) that was dissolved in 40.0 mL of DMF. The mixed solution was stirred for 6 hours at 90 °C. After the mixture was cooled, 100 mL of HCl (1 M) was slowly added to the solution, and the reaction mixture was then stirred at room temperature for 10 minutes. Then, 800 mL of water was added and the mixture was extracted with 50 mL of ethyl acetate three times. The organic layer was collected and dried using Na_2SO_4. After that, the organic solution was concentrated under reduced pressure. The residue was purified by chromatography (silica gel; 95/5 v/v n-hexane/ethyl acetate) and about 1.08 g (59.34% yield) of yellow oily liquid of **(*E*)-NAA** was harvested **(Figure S1)**. ^1H NMR (600 MHz, 298 K, $CDCl_3$) δ 9.85 (d, J = 7.70 Hz, 1H), 8.31 (d, J = 15.72 Hz, 1H), 8.18 (d, J = 8.43 Hz, 1H), 7.95 (d, J = 8.19 Hz, 1H), 7.90 (d, J = 8.11 Hz, 1H), 7.81 (d, J = 7.21 Hz, 1H), 7.65 - 7.60 (m, 1H), 7.60 - 7.55 (m, 1H), 7.53 (t, J = 7.72 Hz, 1H), 6.84 (dd, J = 15.71, 7.70 Hz, 1H) **(Figure S2)**. ^{13}C NMR (151 MHz, 298 K, $CDCl_3$) δ 193.65, 149.32, 133.73, 131.61, 131.17, 130.90, 128.97, 127.27, 126.41, 125.71, 125.47, 122.76 **(Figure S3)**. HR-MS (EI): calculated for $C_{13}H_{10}O$, [M] = 182.0732, found = 182.0730 **(Figure S4)**.

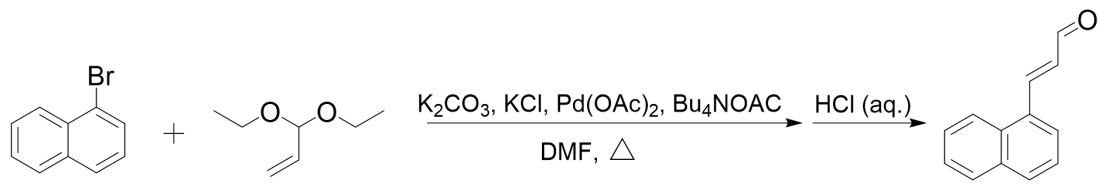

Figure S1. Produce of synthesizing **(*E*)-NAA**.

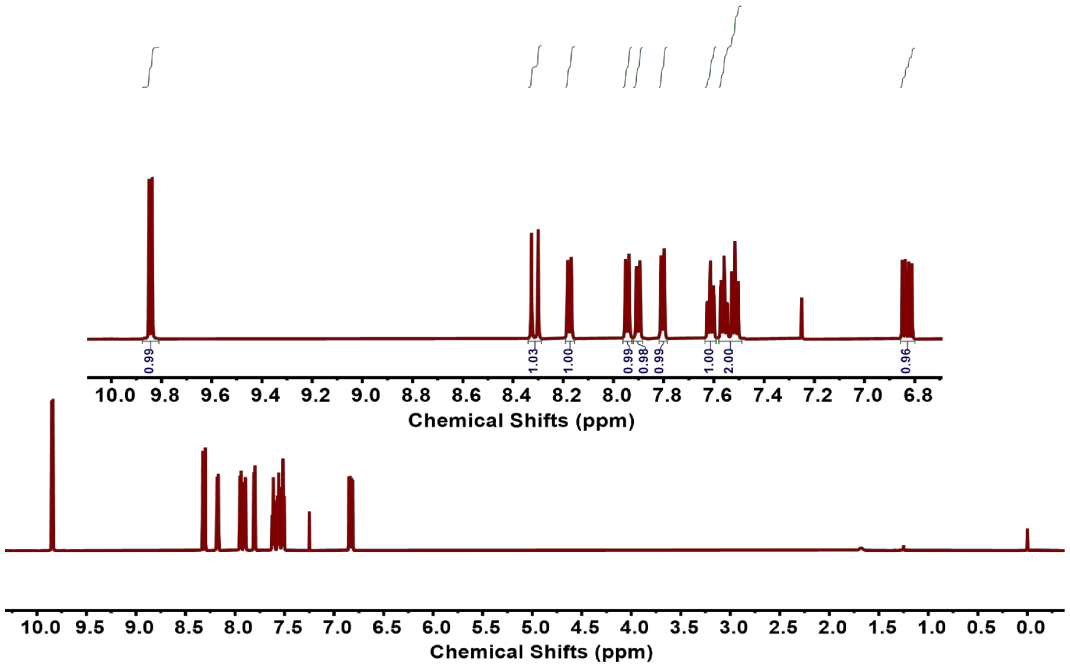

Figure S2. ^{1}H NMR spectrum of **(*E*)-NAA** in $CDCl_3$. The single peak at around 7.26 ppm is due to $CDCl_3$. Inset: magnified region from 6.8 to 9.9 ppm.

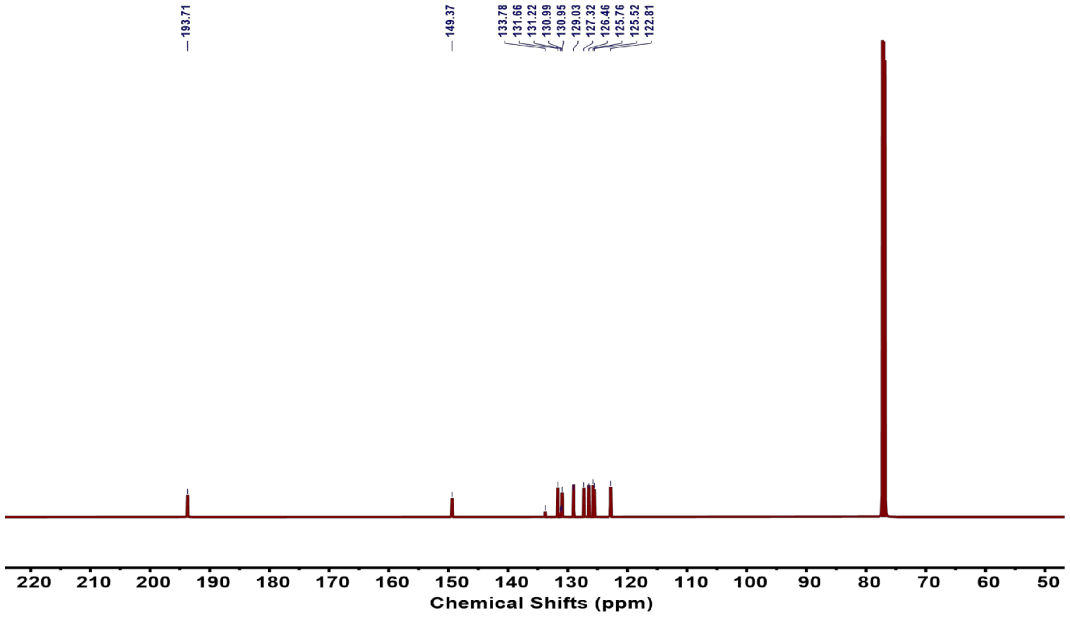

Figure S3. ^{13}C NMR spectrum of **(*E*)-NAA** in $CDCl_3$. The multiple intense peaks at around 78 ppm are due to $CDCl_3$.

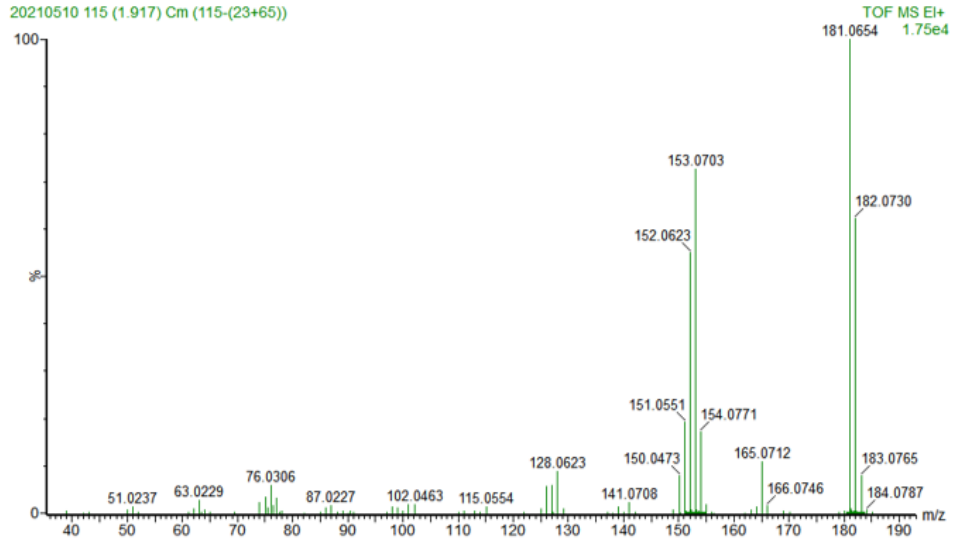

Figure S4. HR-EI-MS spectrum of **(*E*)-NAA**.

Synthesis of the compound (*E*)-NAPT:

Barbituric acid (0.64 g, 4.99 mmol) and **(*E*)-NAA** (0.91 g, 4.99 mmol) were added to a round-bottomed flask containing 20 mL of ethanol and refluxed at 78°C for 5 h. At the end of the reaction, it was cooled down to room temperature and the solid was filtered out, washed with ethanol and then placed in a vacuum oven at 45°C. After leaving it to dry overnight an orange-yellow powder was obtained (85.82% yield) **(Figure S5)**.^{1}H NMR (400 MHz, 298 K, DMSO-d_6) δ 11.28 (d, J = 1.9 Hz, 1H), 11.23 (s, 1H), 8.70 (d, J = 15.2 Hz, 1H), 8.59 (dd, J = 15.1, 11.4 Hz, 1H), 8.50 (d, J = 8.4 Hz, 1H), 8.30 (d, J = 11.4 Hz, 1H), 8.08 (d, J = 8.2 Hz, 1H), 8.06 – 7.98 (m, 2H), 7.71 – 7.58 (m, 3H) **(Figure S6)**.^{13}C NMR (101 MHz, 298K, DMSO-d_6) δ 163.70, 163.55, 154.46, 150.86, 149.37, 133.97, 132.53, 132.04, 131.60, 129.29, 127.81, 126.99, 126.85, 126.40, 125.94, 123.83, 116.27 **(Figure S7)**. HR-MS (ESI): calculated for: $C_{17}H_{12}N_2O_3$, [M] = 292.0848, found = 292.0820 **(Figure S8)**.

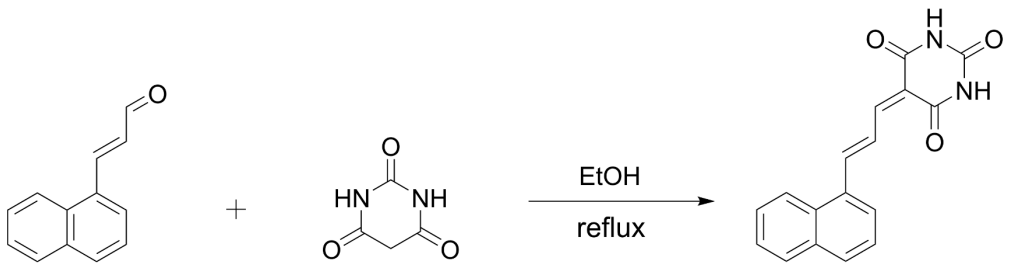

Figure S5. Produces of synthesizing **(*E*)-NAPT**.

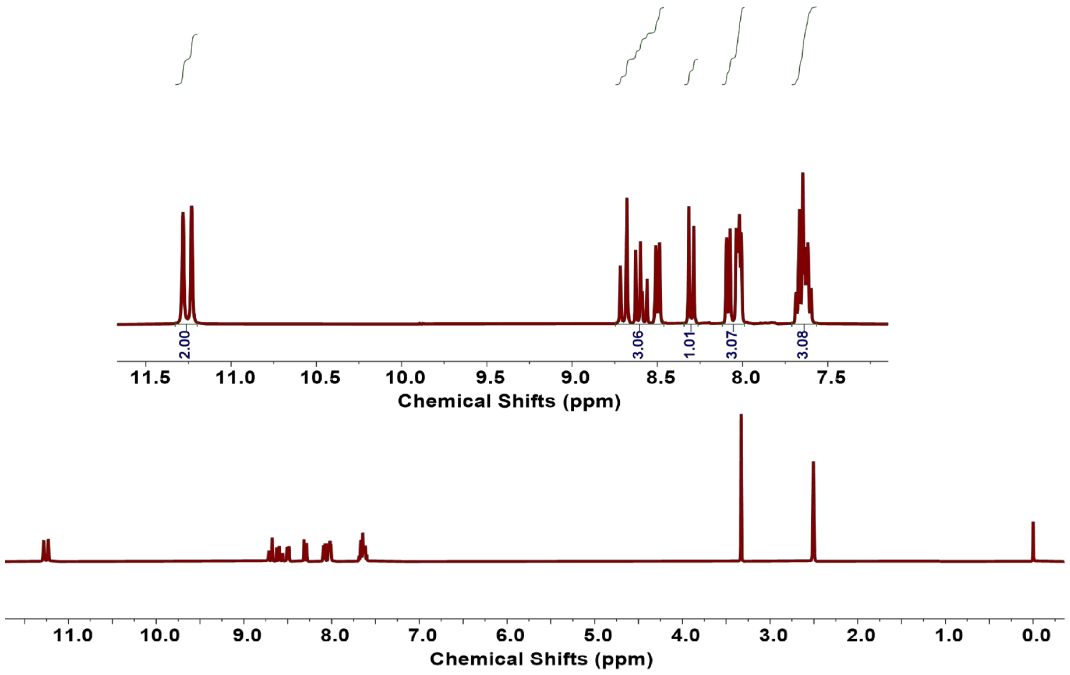

Figure S6. ^{1}H NMR of **(*E*)-NAPT**. The peak near 2.5 ppm is from solvent, the peak near 3.33 is due to residue water. Inset: The enlarged region between 7.5 and 11.5 ppm (DMSO-d_6 as solvent).

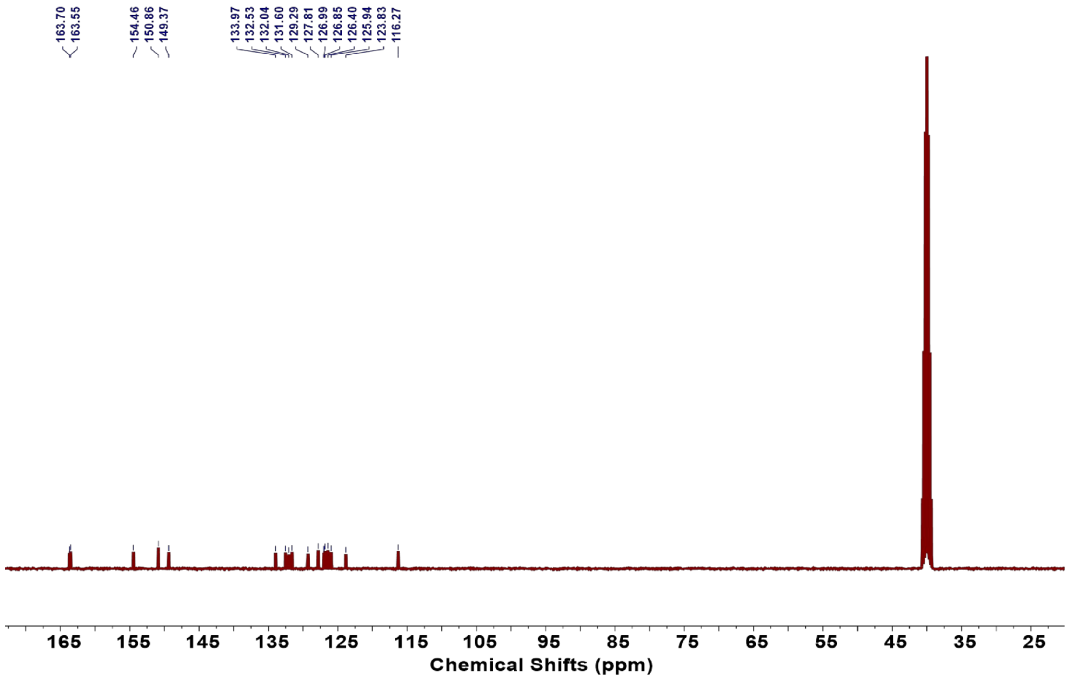

Figure S7. ^{13}C NMR spectrum of **(*E*)-NAPT**. The peak around 39.52 ppm is due to solvent (DMSO-d_6 as solvent).

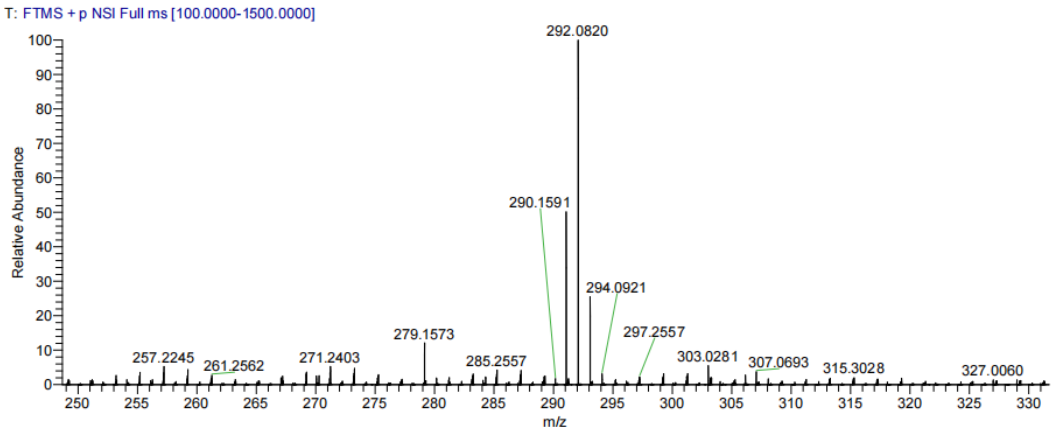

Figure S8. HR-MS (ESI) spectrum of **(*E*)-NAPT**.

Table S5. Packing index of four polymorphs.

	Form A	Form B	Form C	Form D
Packing Index	75.5%	52.8%	71.5%	71.1%

Table S6. Comparative stimuli-responsive ability of four polymorphs.

	Form A	Form B	Form C	Form D
Fumigation	—	✓	—	✓
Heating	✓	✓	—	—
Photochemical reactivity	✓	—	—	—

"✓" indicates stimulus responsiveness while "—" means non-responsiveness.

Table S7. Comparative characterization of four polymorphs.

	color	morphology	λ_{em}	QY
Form A	dark red	needle	680 nm	0.476%
Form A-H	orange	/	587 nm	7.51%
Form A-H-W	dark red	/	678 nm	0.503%
Form A after irradiation	orange-yellow	/	595 nm	0.541%
Form B	orange-yellow	needle	635 nm	6.80%
Form B-W	dark red	/	678 nm	0.494%
Form B-H	dark red	/	690 nm	3.83%
Form C	red	needle	690 nm	4.88%
Form D	yellow	block	587 nm	8.33%
Powder	orange-yellow	/	590 nm	7.32%

λ_{em} means the maximum wavelength of emission with the 365 nm excitation, while QY means the quantum yield.

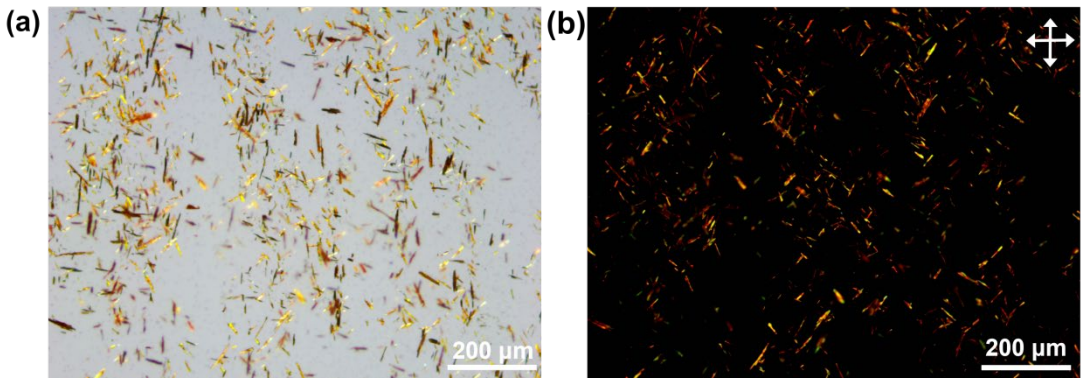

Figure S9. (a) Optical microscope images and (b) cross-polarized microscope images of (***E***)**-NAPT** polycrystals.

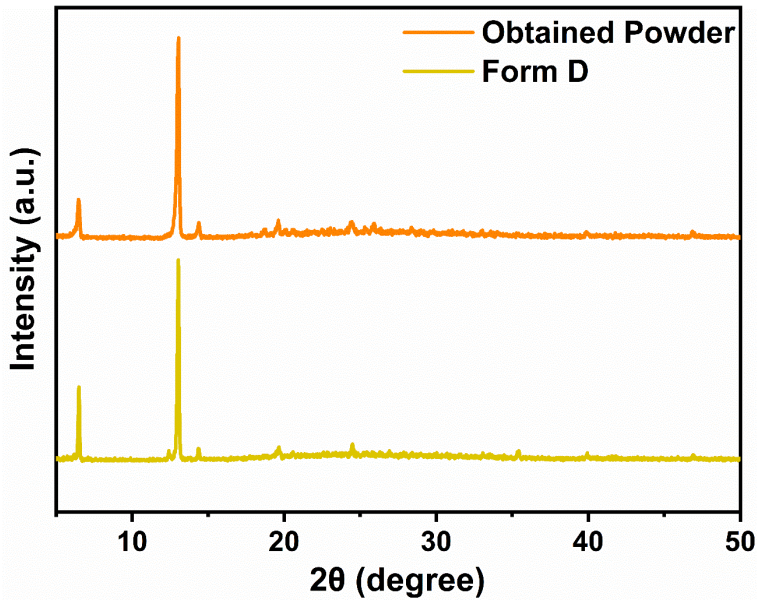

Figure S10. The stacked PXRD pattern of the obtained powder **(*E*)-NAPT** and Form D.

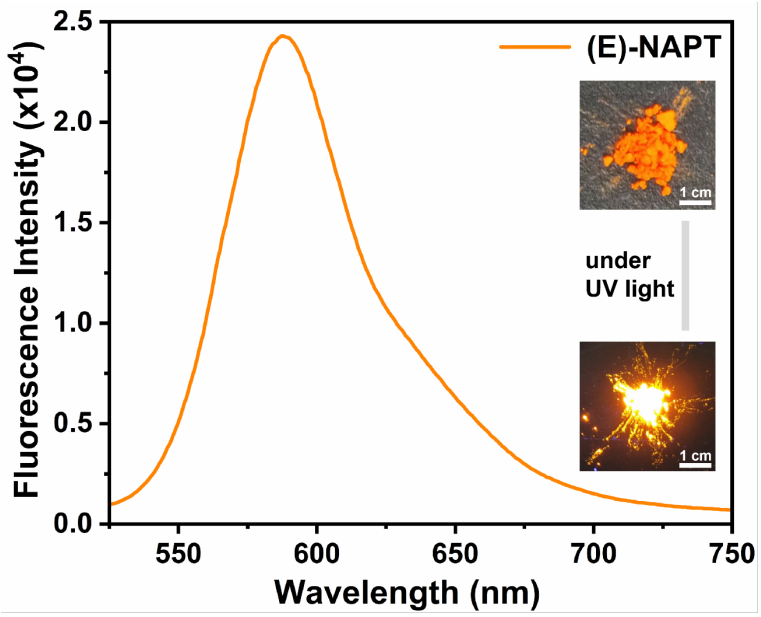

Figure S11. Emission spectra of synthesized **(*E*)-NAPT** solids. The inset shows the powder morphology of **(*E*)-NAPT,** and upon UV light.

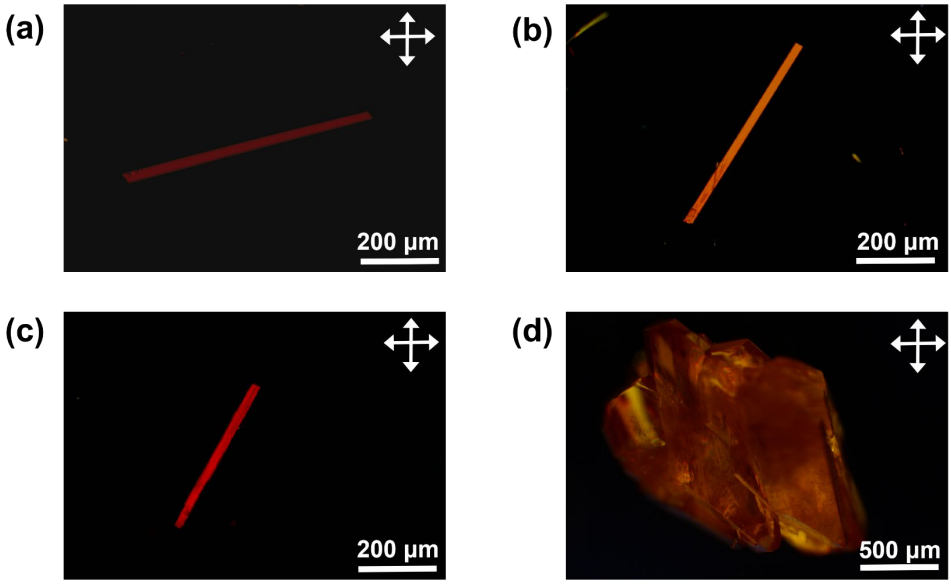

Figure S12. Cross-polarized microscope images of (a) Form A, (b) Form B, (c) Form C, and (d) Form D.

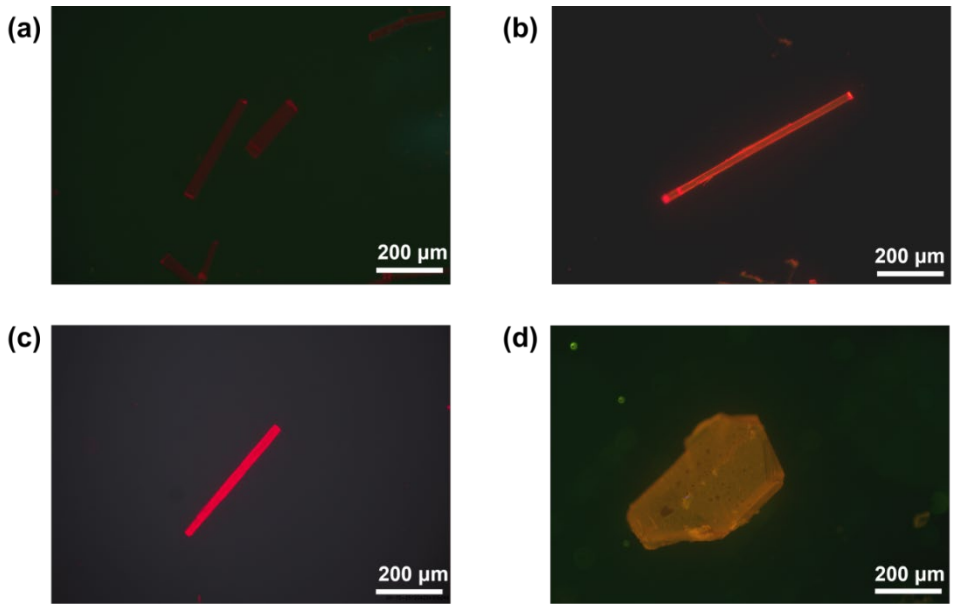

Figure S13. Optical microscope image of (a) Form A, (b) Form B, (c) Form C, and (d) Form D under UV light.

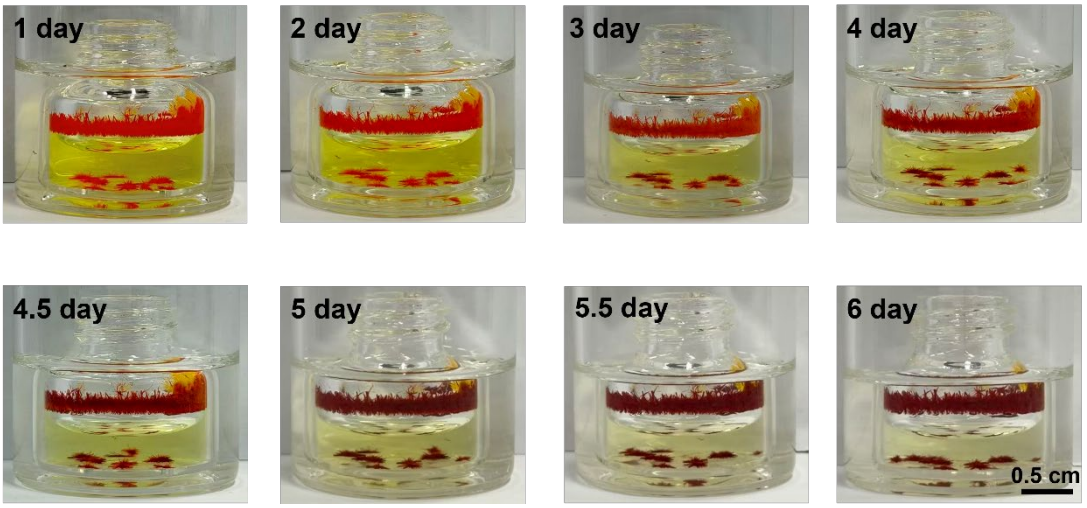

Figure S14. Daily photographs showing the transformation of Form B to Form C via prolonged solvent evaporation.

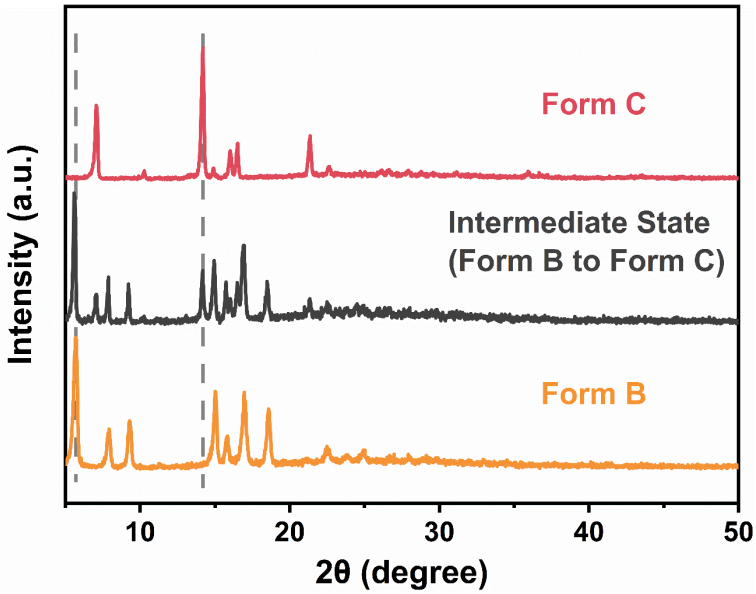

Figure S15. The stacked PXRD patterns of the Form B, intermediate state (Form B to Form C, Day 4) and Form C.

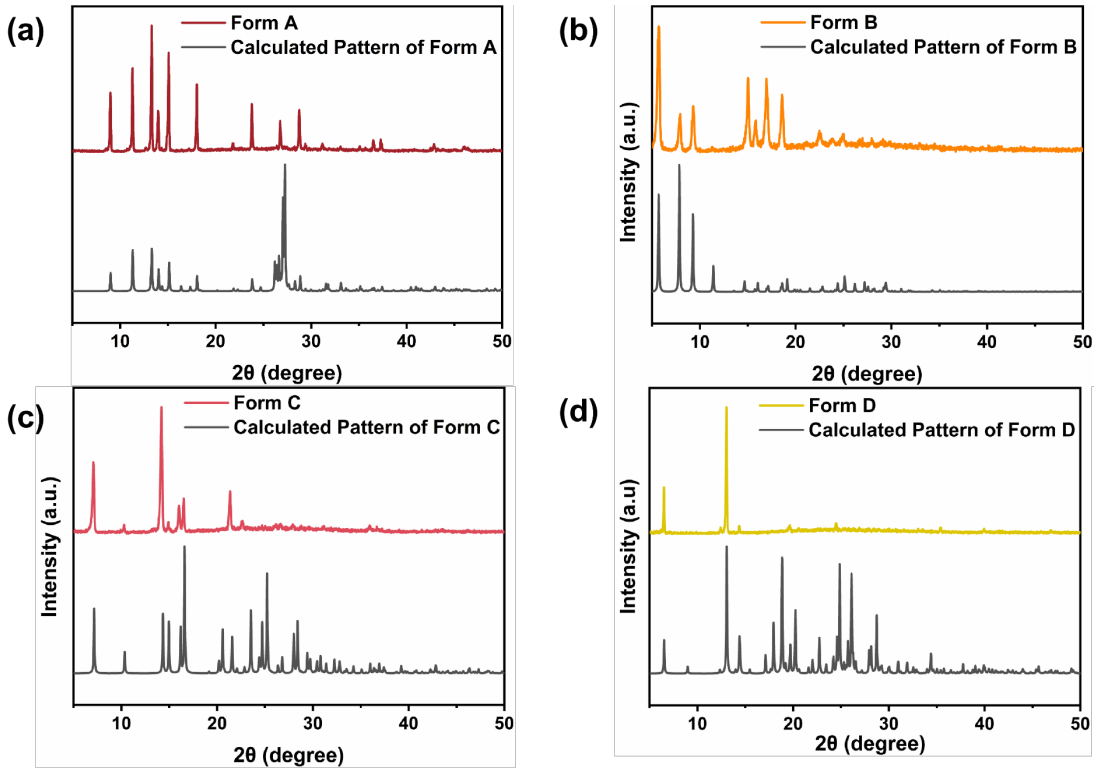

Figure S16. The stacked PXRD patterns of the (a) Form A, (b) Form B, (c) Form C and (d) Form D and the calculated pattern, respectively.

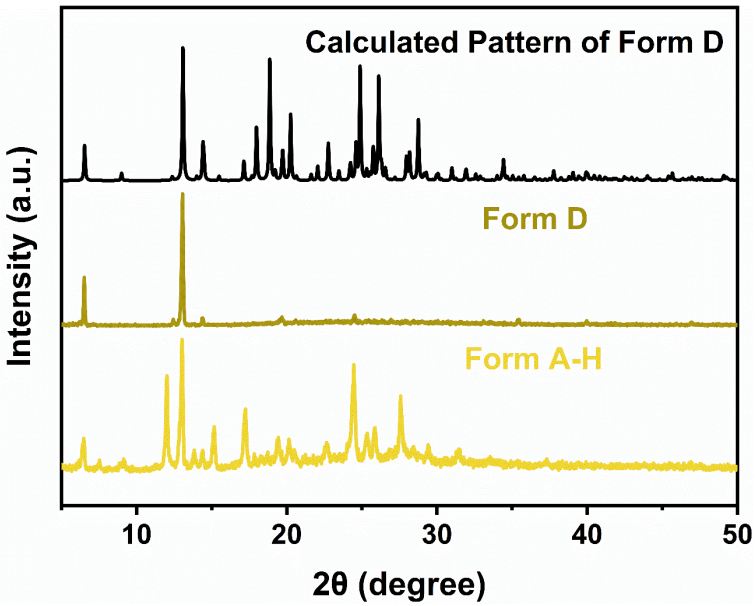

Figure S17. The stacked PXRD patterns of Form D, Form A-H and calculated pattern of Form D.

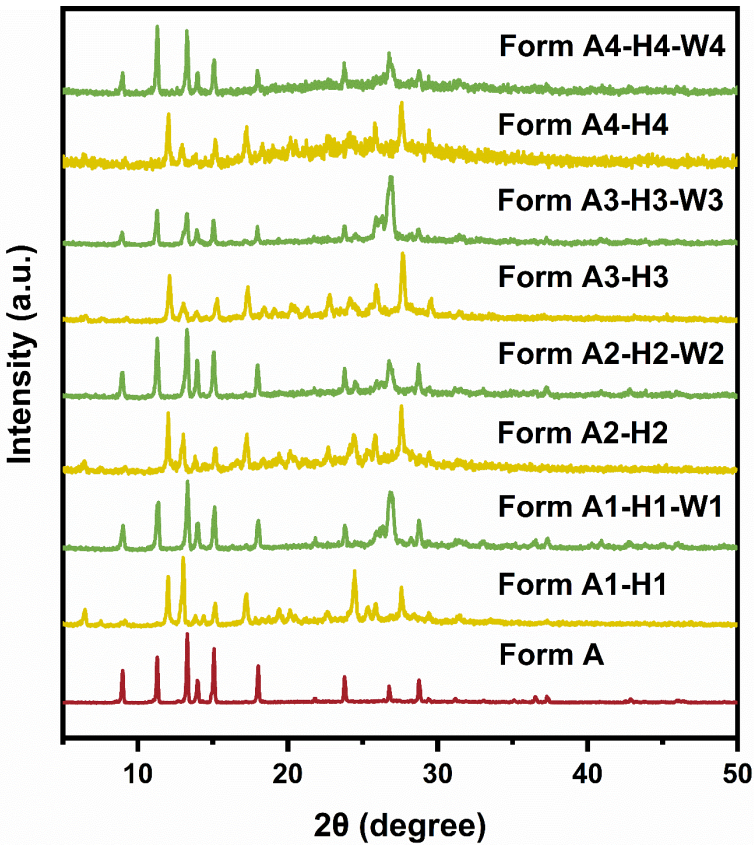

Figure S18. Four cycles of PXRD patterns of Form A, Form A-H, and Form A-H-W.

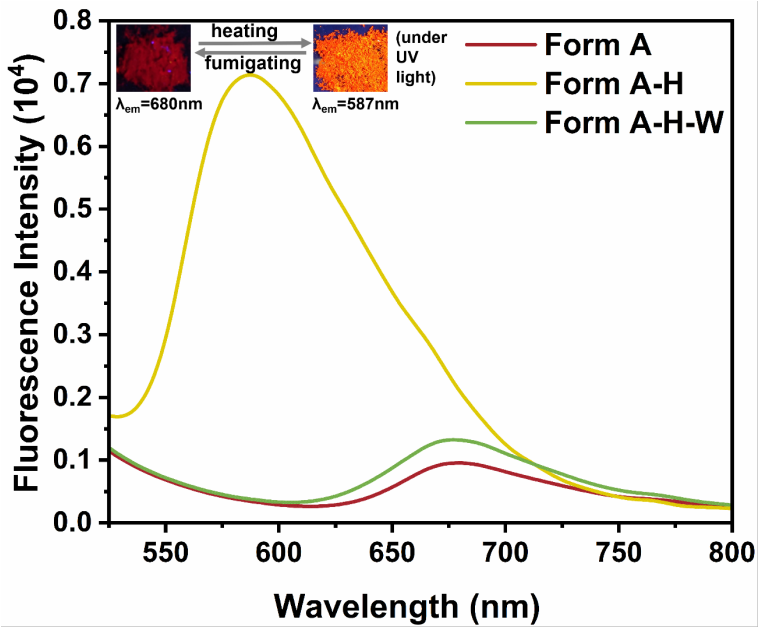

Figure S19. Emission spectra and luminescence images of Form A, Form A-H and Form A-H-W.

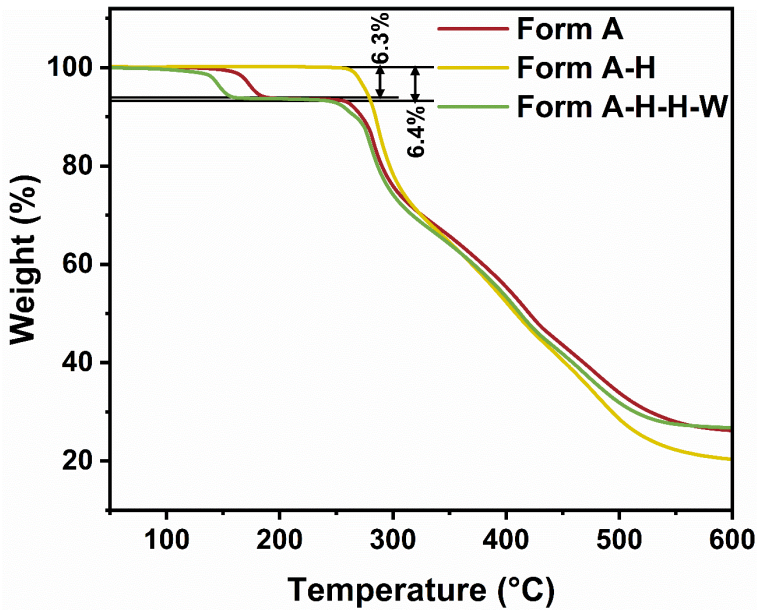

Figure S20. The TGA curves of Form A, Form A-H, and Form A-H-W. The initial weight-loss temperatures for Form A and Form A-H-W are 120°C and 100°C, respectively.

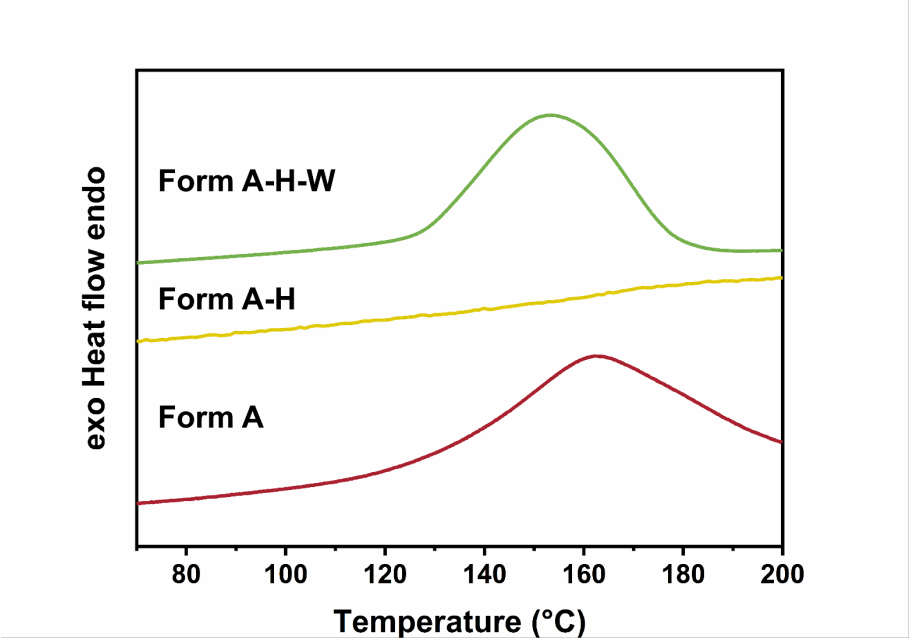

Figure S21. DSC curve of Form A, Form A-H, and Form A-H-W.

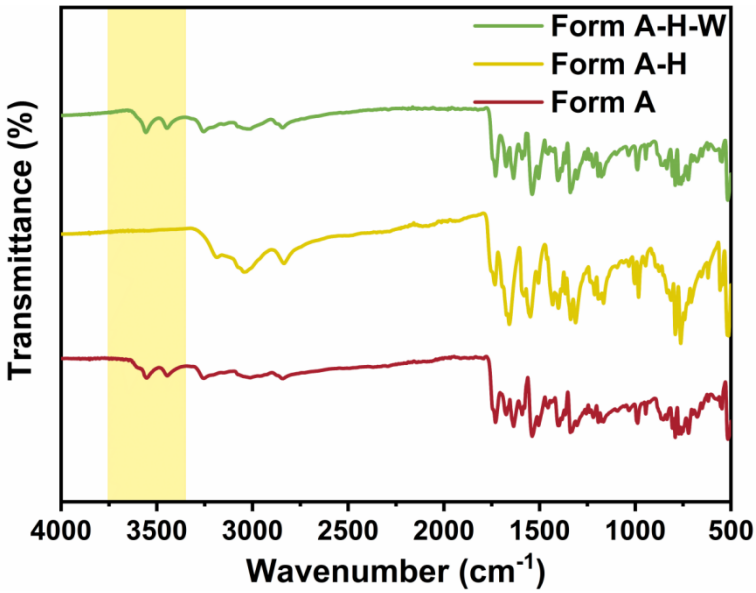

Figure S22. The FT-IR spectra of Form A, Form A-H, and Form A-H-W.

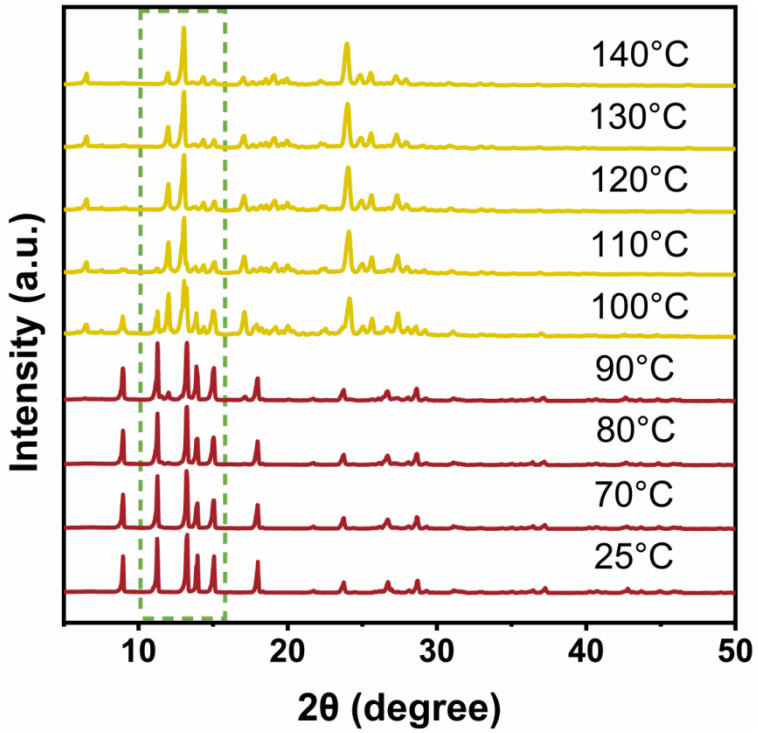

Figure S23. Temperature-dependent PXRD patterns of Form A from 25°C to 140°C.

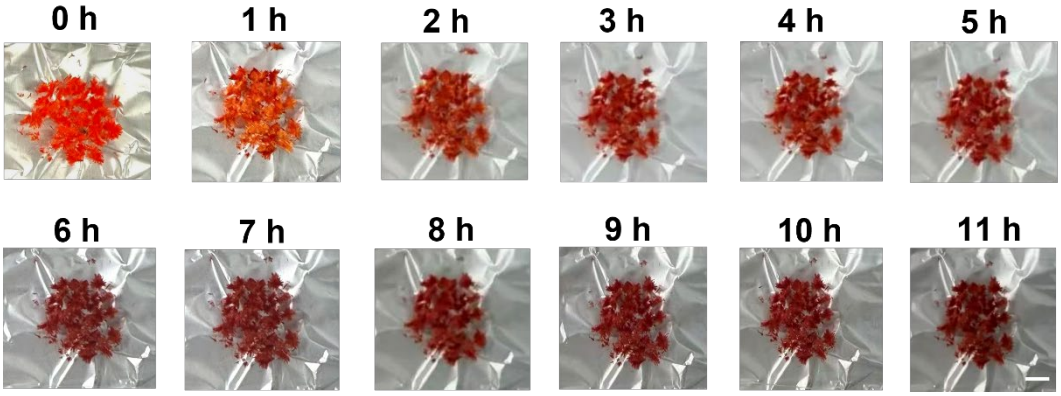

Figure S24. The digital photos show the progressive transformation of Form B into Form B-W upon fumigation. Scale bar: 0.5 cm.

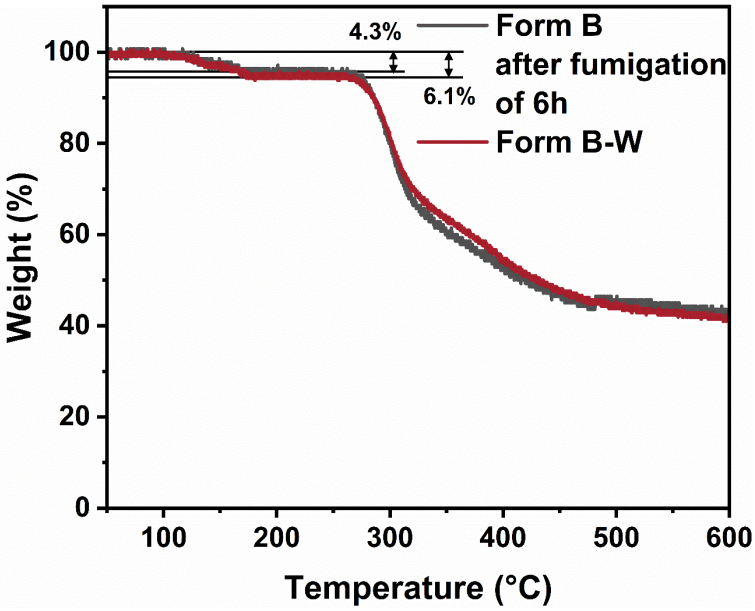

Figure S25. The TGA curves of Form B after fumigation of 6 h and Form B-W, showing an increase in water content from 4.3% to 6.1%.

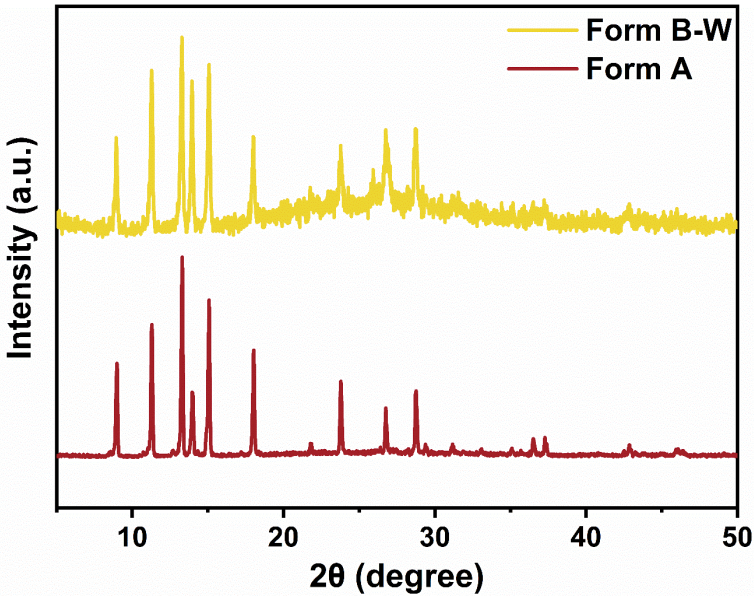

Figure S26. The PXRD patterns of Form A and Form B-W.

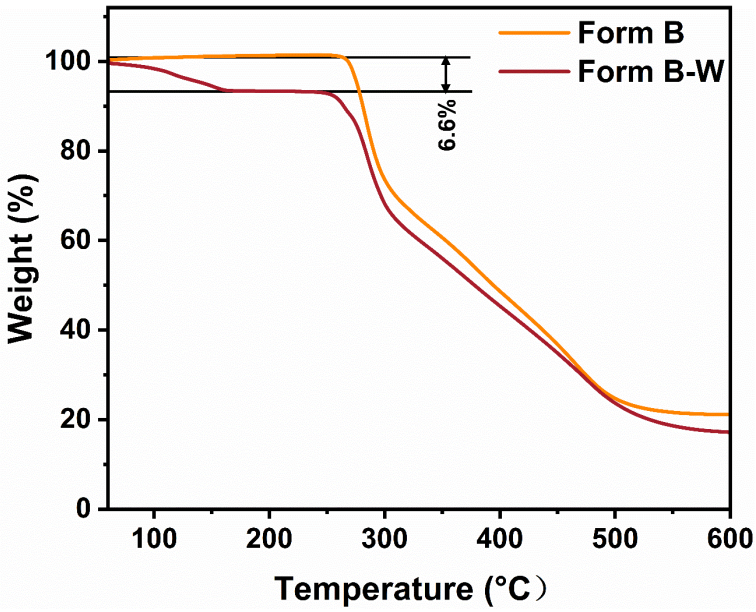

Figure S27. The TGA curves of Form B and Form B-W.

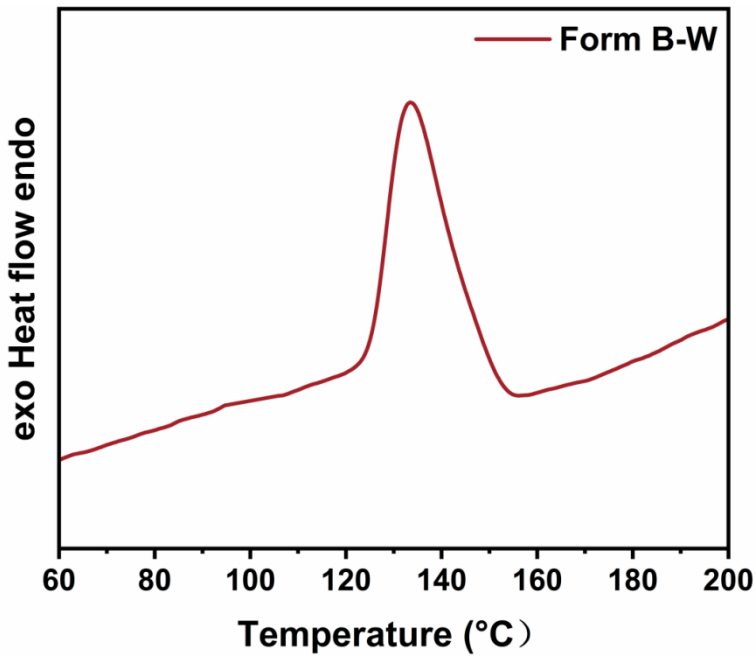

Figure S28. DSC curve of Form B-W.

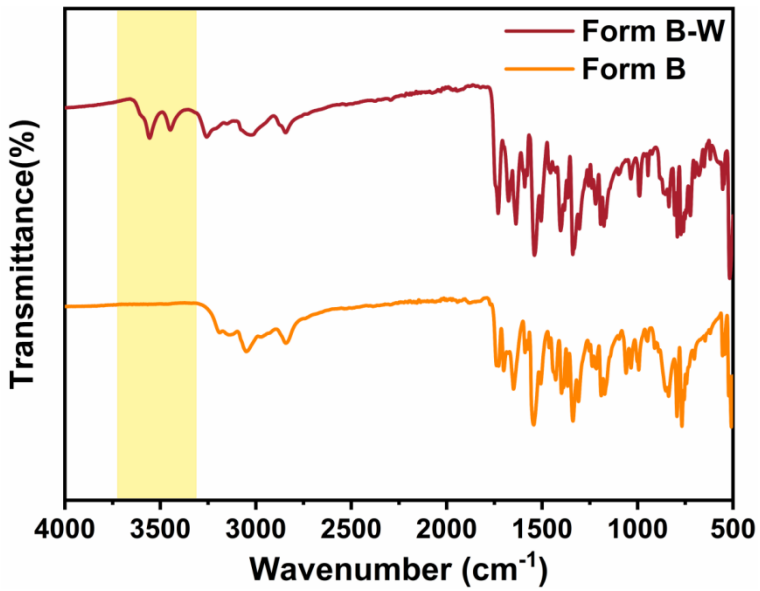

Figure S29. The FT-IR of Form B and Form B-W.

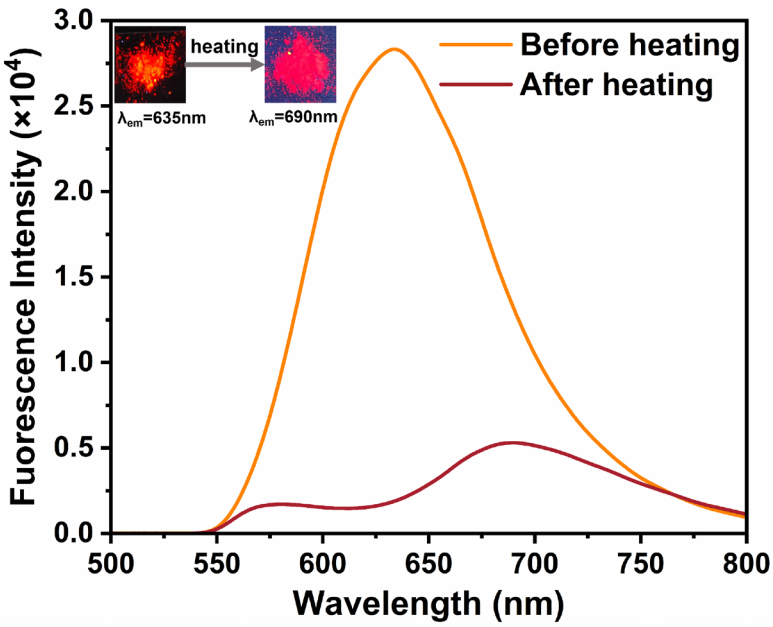

Figure S30. Emission spectra and luminescence images of Form B before and after heating.

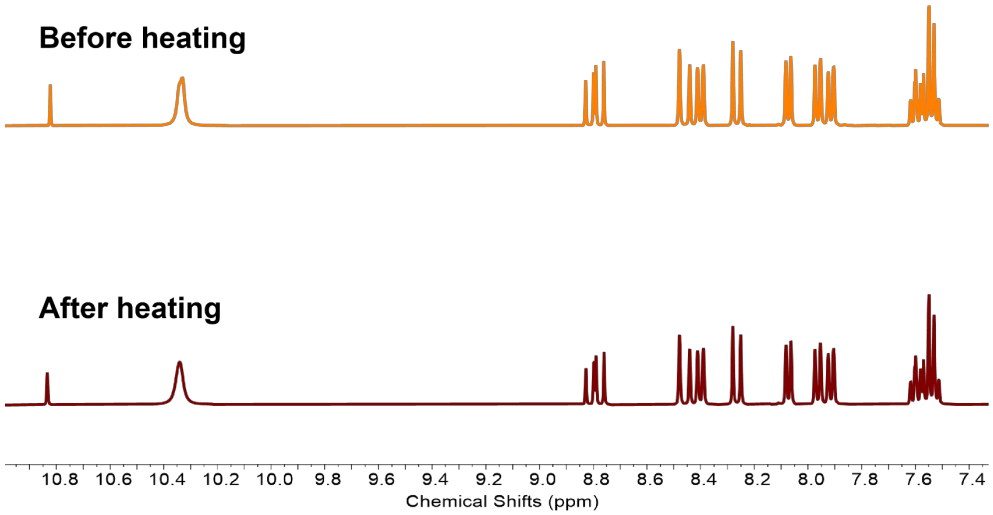

Figure S31. ^{1}H NMR spectra of Form B before and after heating.(THF-d_8 as the solvent).

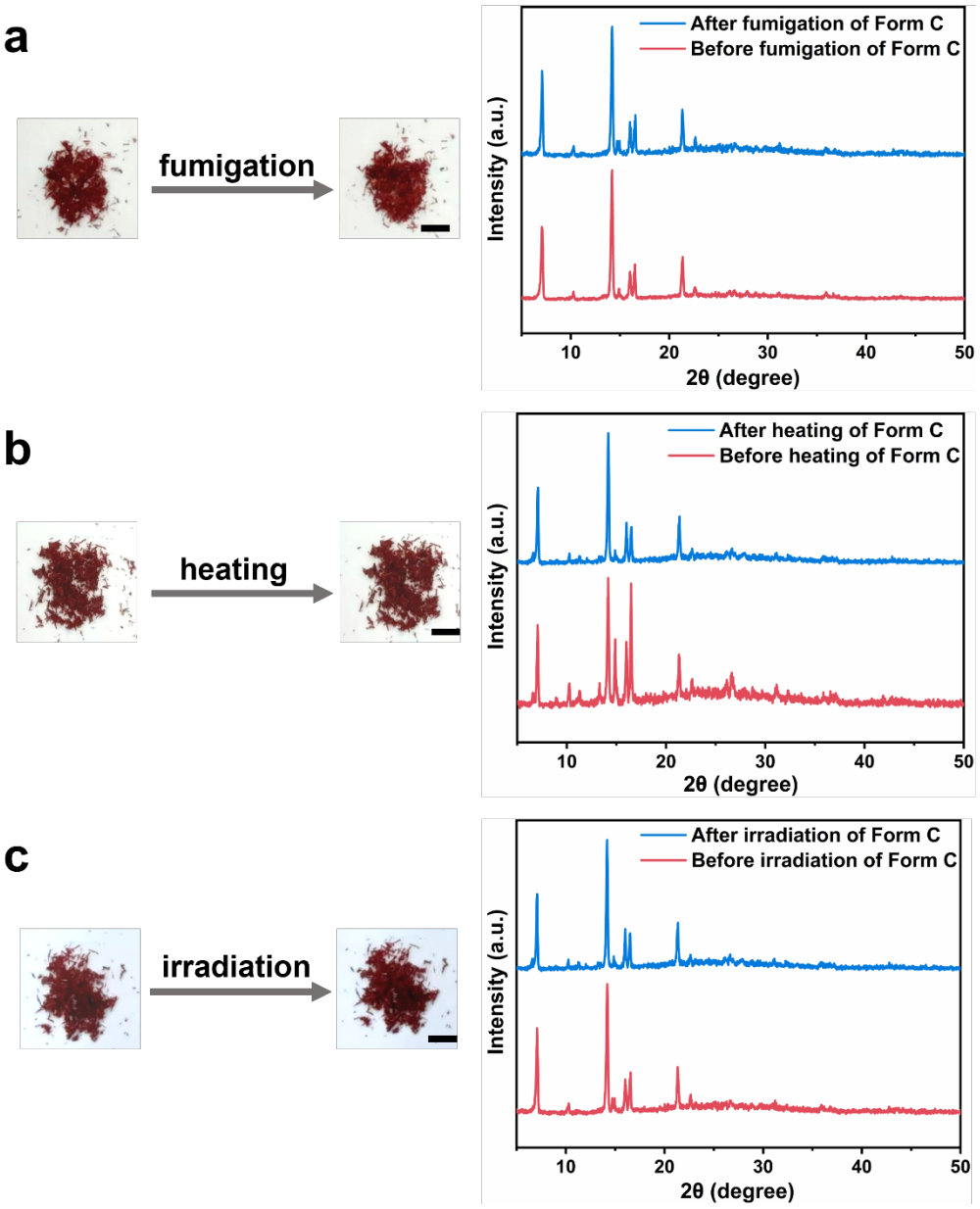

Figure S32. The digital photos and the stacked PXRD patterns of Form C before and after (a) fumigation, (b) heating, and (c) irradiation. Scale bars: 0.5 cm.

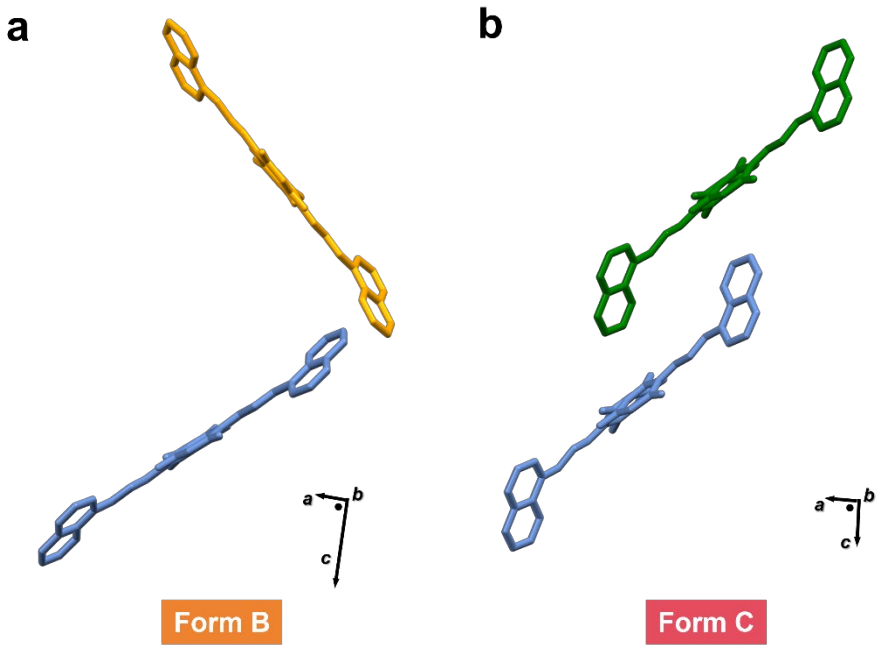

Figure S33. Side view of typical packing mode of (a) Form B and (b) Form C. The molecular packing in Form B is characterized by a crisscross arrangement, in contrast to the parallel alignment observed in Form C.

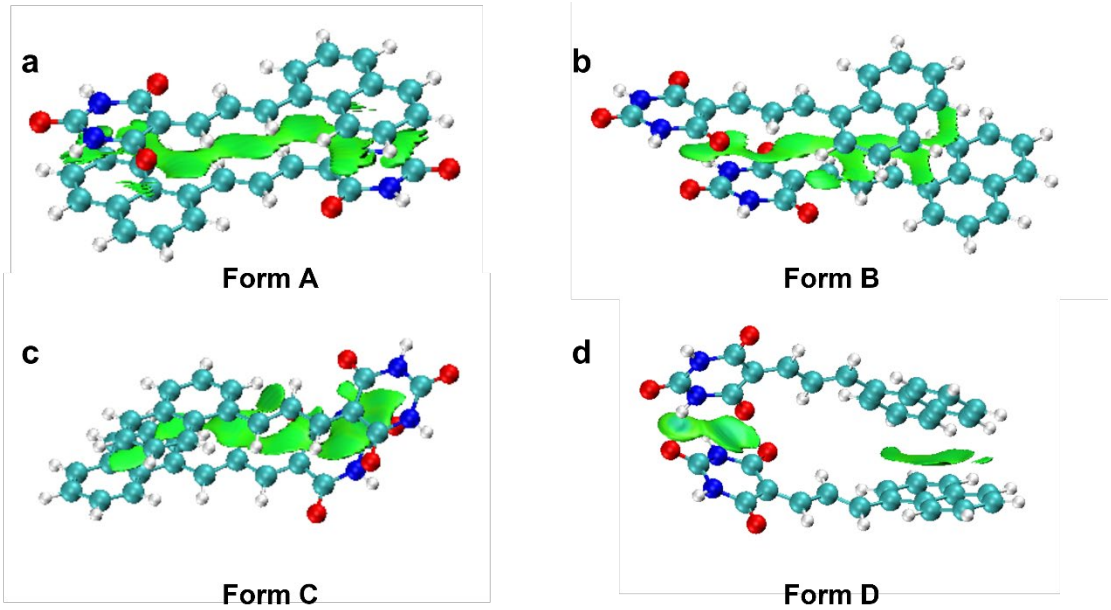

Figure S34. IGMH (independent gradient model based on Hirshfeld partition, δg^{inter}=0.005) analysis of the main noncovalent interactions of (a) Form A, (b) Form B, (c) Form C, and (d) Form D.

Table S8. Interaction energy and its energy decomposition of four polymorphs.

	E_{int}	E_{els}	E_{ex}	E_{orb}	E_{disp}
Form A	-20.31	-9.74	24.60	-3.00	-32.44
Form B	-18.43	-9.90	23.63	-3.31	-28.86
Form C	-17.52	-10.98	26.10	-3.54	-29.10
Form D	-15.52	-13.56	22.60	-5.23	-19.33

Unit: kcal mol^{-1}.

E_{int} = Interaction Energy, E_{els} = Electrostatic Energy, E_{ex} = Exchange Energy, E_{orb} = Orbital Interaction Energy, E_{disp} = Dispersion Energy.

The strength of π-π interactions is dominated by the dispersion energy (E_{disp}).

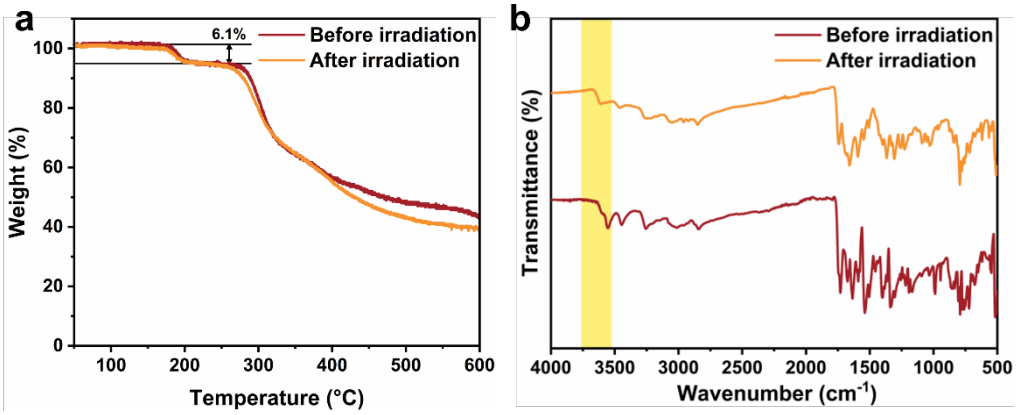

Figure S35. (a) TGA and (b) the FT-IR spectrum of Form A before and after irradiation, confirming the existence of water.

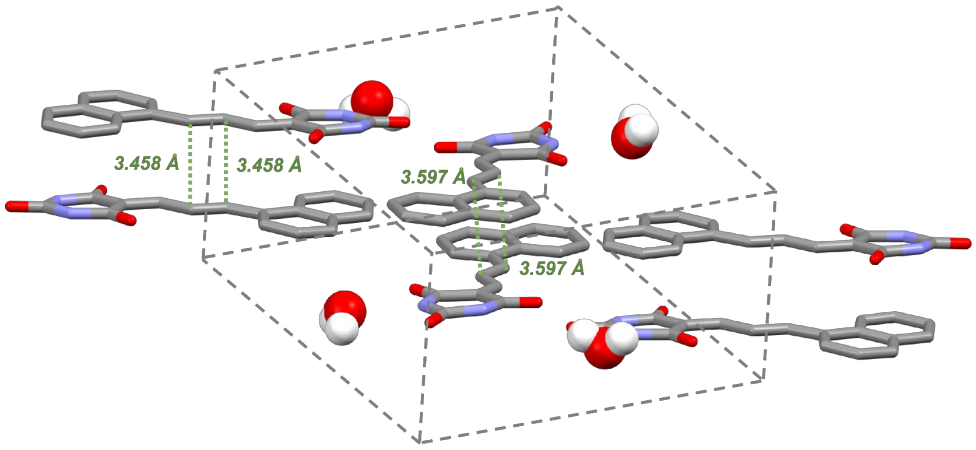

Figure S36. Representative packing mode of Form A. The green dashed arrows indicate the intermolecular distance between two vinyl groups that allow photodimerization.

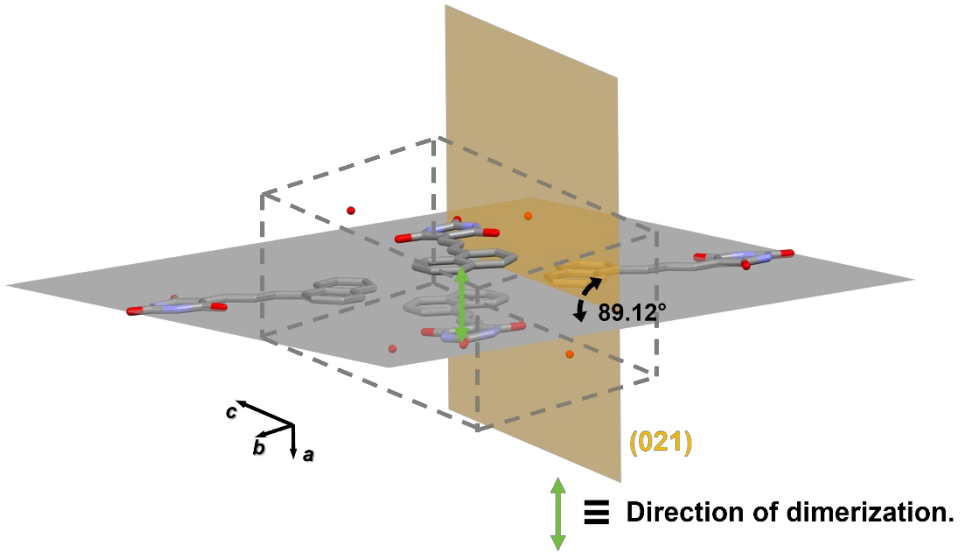

Figure S37. The spatial orientation of the dominant crystal plane (021) relative to the molecular plane within the unit cell of Form A. The red plane corresponds to the (021) plane, while the grey plane denotes the plane of the molecule in its planar conformation. The dihedral angle between these two planes is 89.12°, indicating that they are effectively perpendicular. Consequently, the preferred direction of crystal growth is orthogonal to the molecular plane and parallel to the axis of dimerization. This suggests that the [2+2] photodimerization in Form A proceeds along the direction of preferred crystal growth.

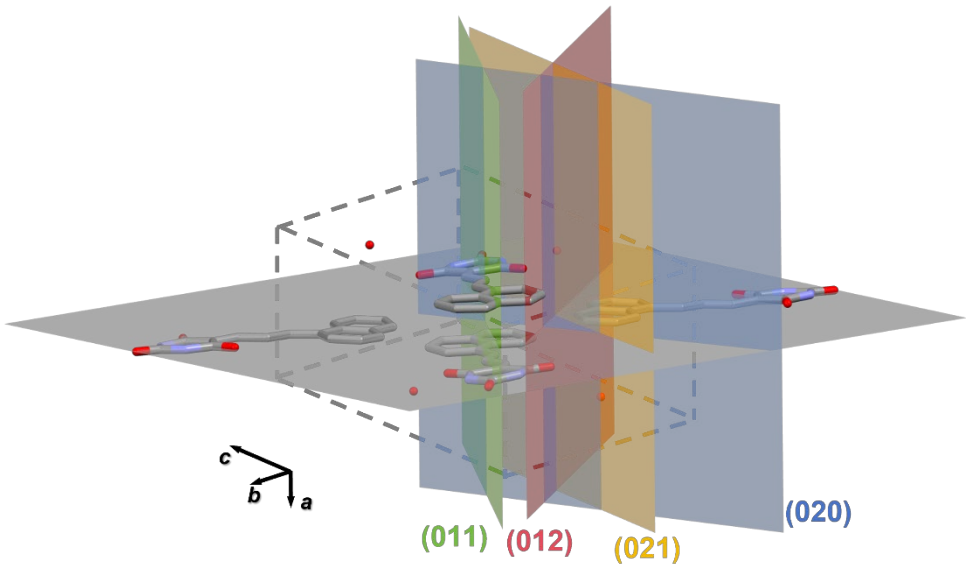

Figure S38. The major crystallographic planes are perpendicular to the molecular stacking plane and align with the direction of molecular dimerization.

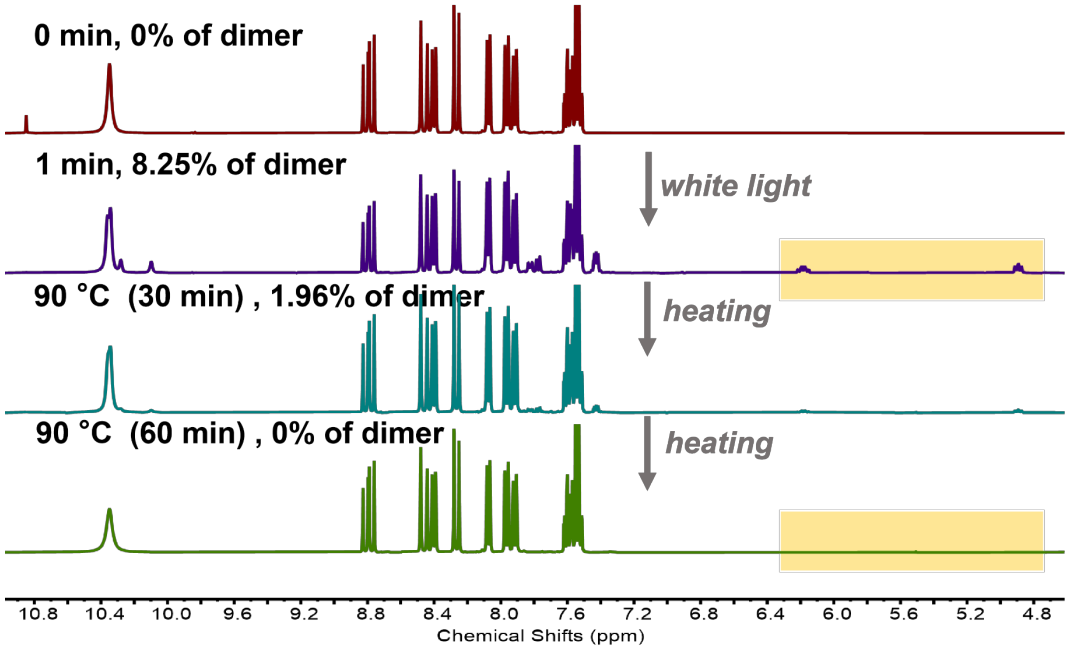

Figure S39. ^{1}H NMR spectra of Form A after being irradiated and heating treatments when the conversion rate is low (THF-d_8 as the solvent).

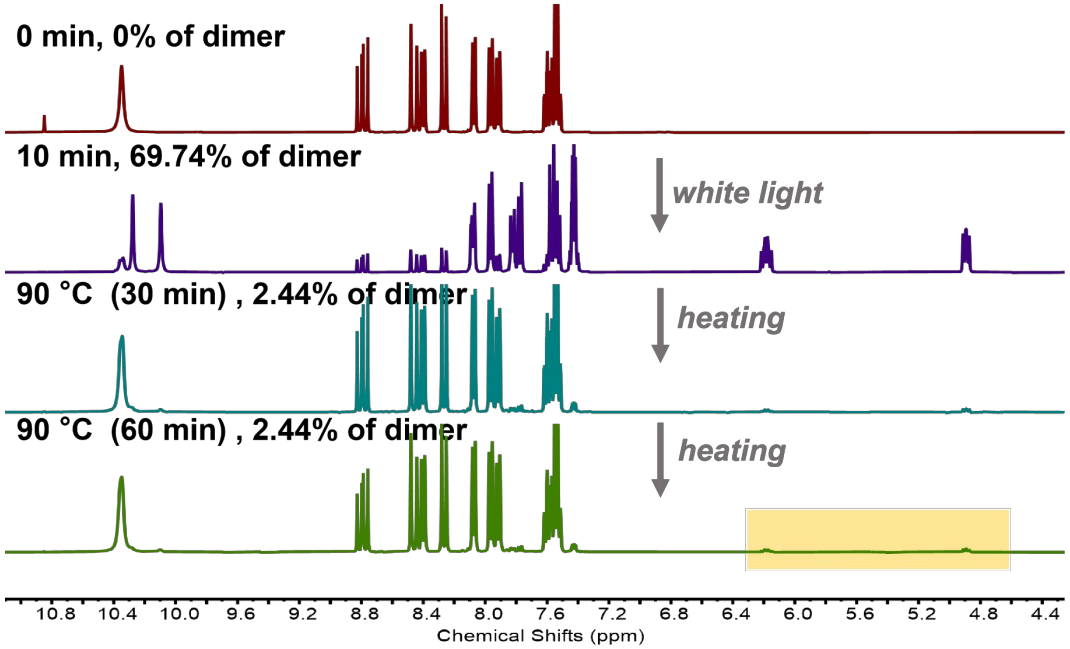

Figure S40. ^{1}H NMR spectra of Form A after being irradiated and heating treatments when the dimer conversion rate is more higher (THF-d_8 as the solvent).

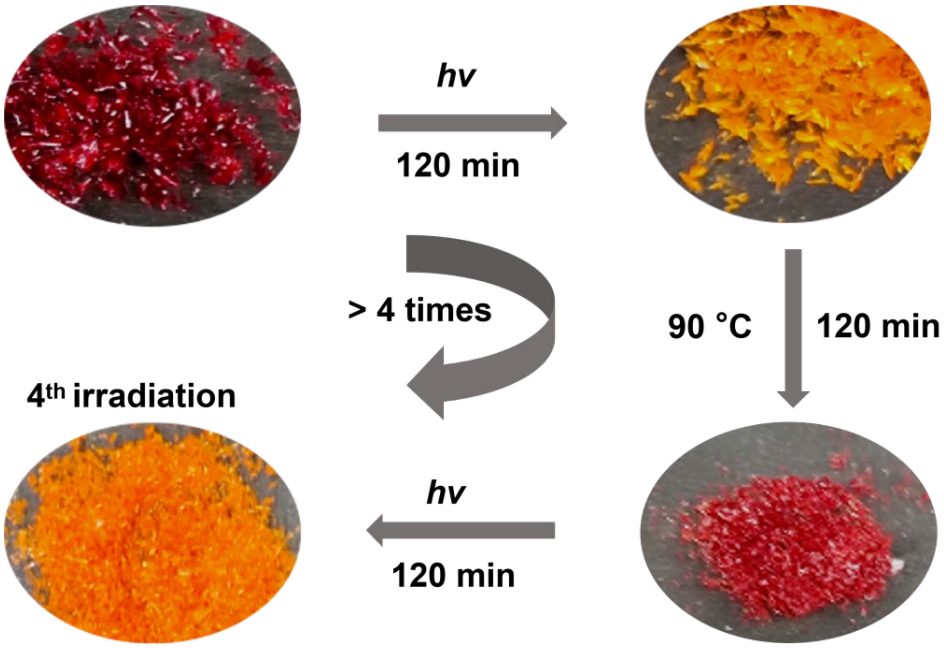

Figure S41. Cycling processes of Form A under white irradiation and heating.

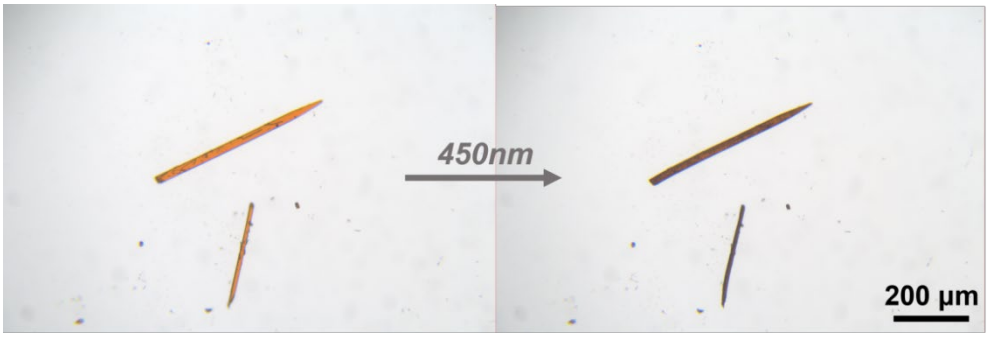

Figure S42. Optical microscope images of Form B exhibit slight bending behavior under visible light irradiation.

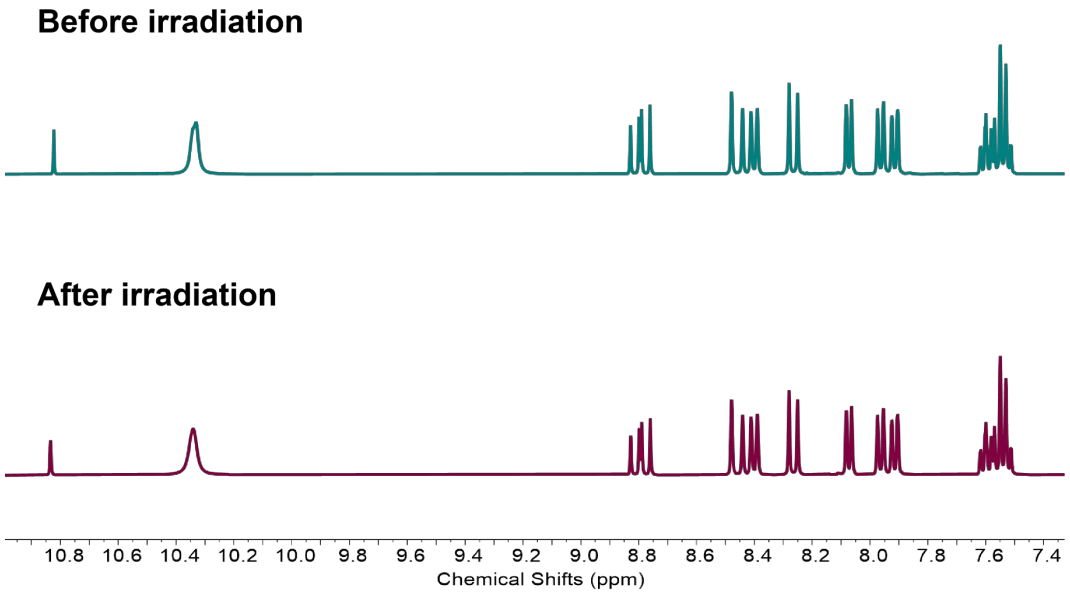

Figure S43. ^{1}H NMR spectra of Form B before and after irradiation. (THF-d_8 as the solvent).

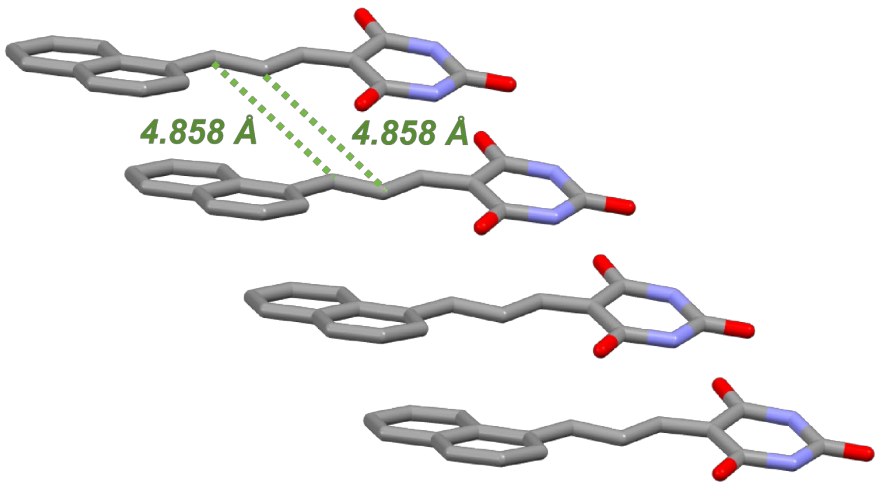

Figure S44. Representative packing mode of Form B. The green dashed arrows indicate the intermolecular distance between two vinyl groups that allows no photodimerization.

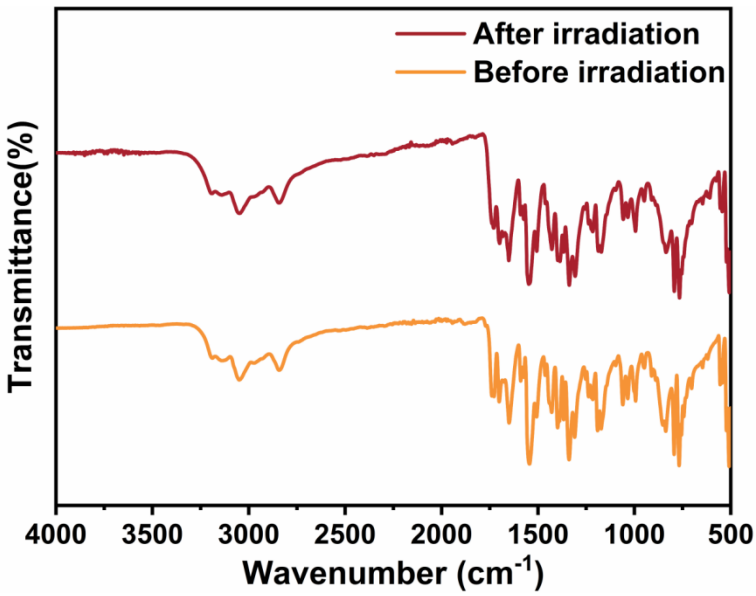

Figure S45. The FT-IR of Form B before and after irradiation.

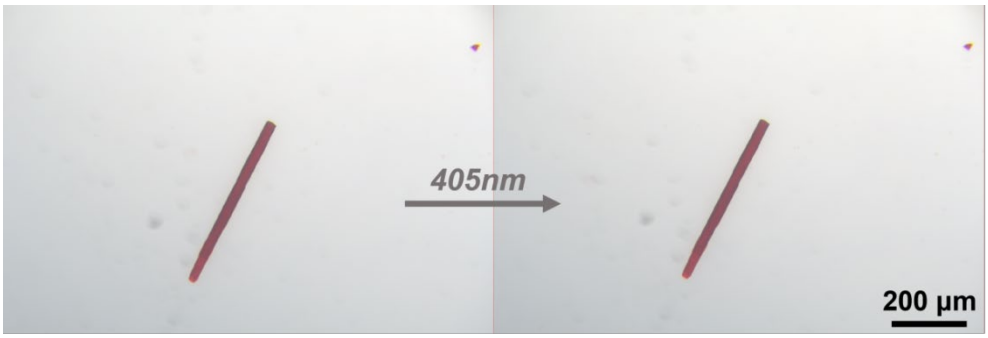

Figure S46. Optical microscope images of Form C exhibiting no change under visible light irradiation.

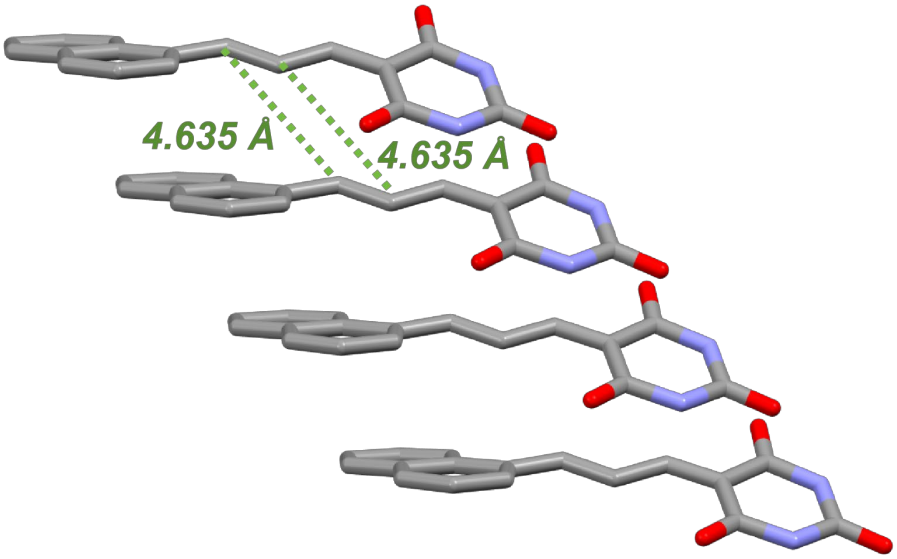

Figure S47. Representative packing mode of Form C. The green dashed arrows indicate the intermolecular distance between two vinyl groups that allows no photodimerization.

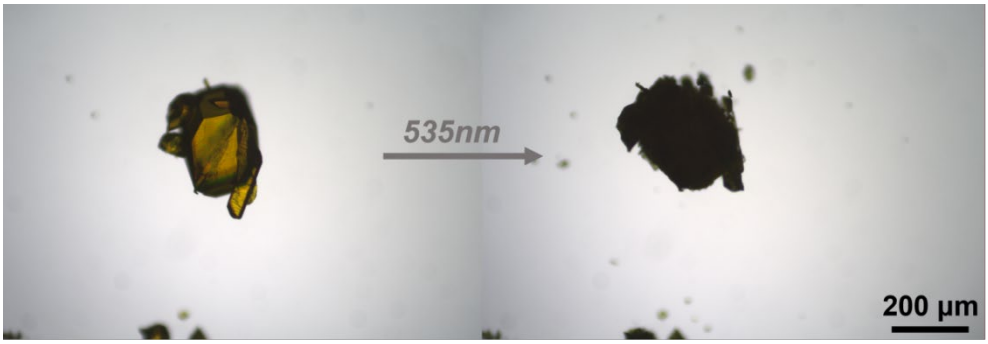

Figure S48. Optical microscope images of Form D exhibiting fragmentation under visible light irradiation.

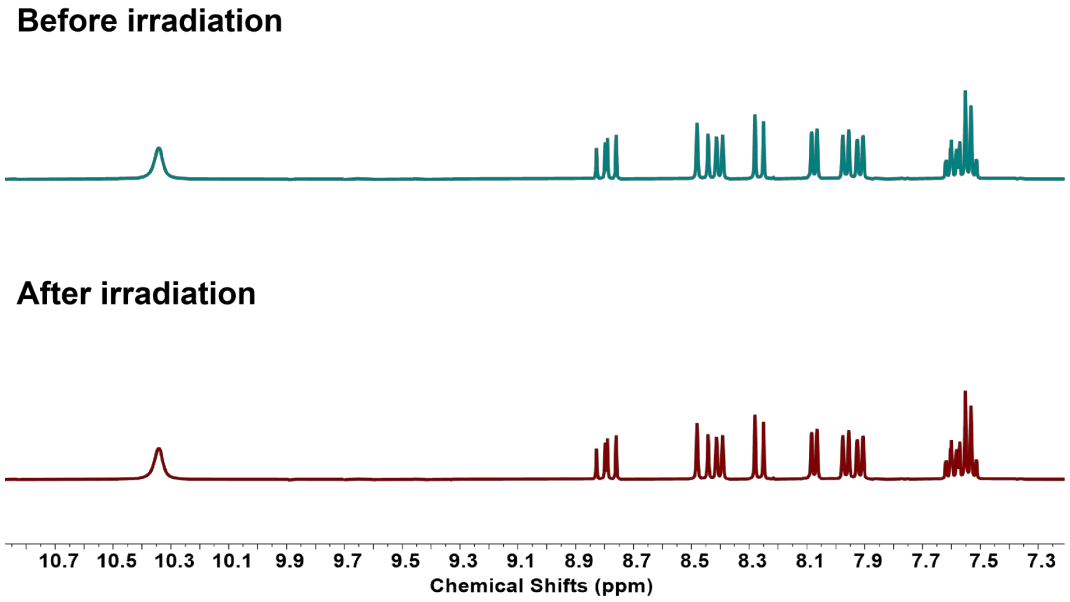

Figure S49. ^{1}H NMR spectra of Form D before and after irradiation. (THF-d_8 as the solvent).

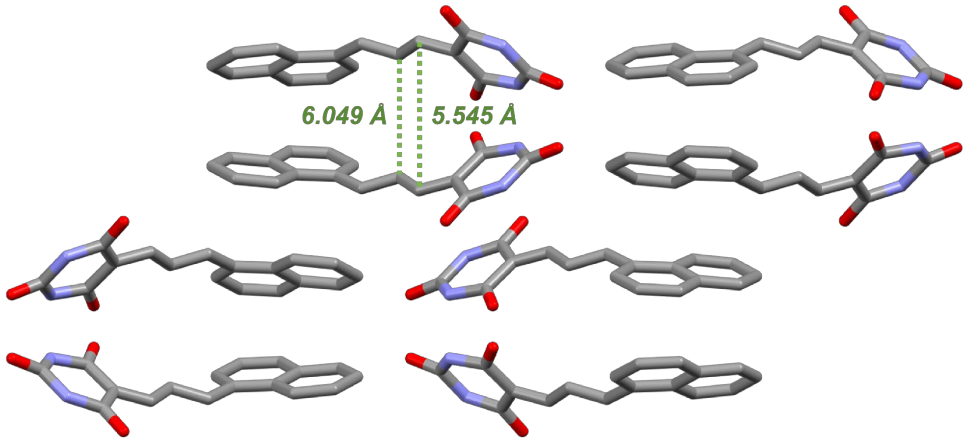

Figure S50. Representative packing mode of Form D. The green dashed arrows indicate the lack of parallel alignment between reactive olefin pairs, which precludes photodimerization.

Figure S51. The digital photos of Form B-W before and after irradiation.

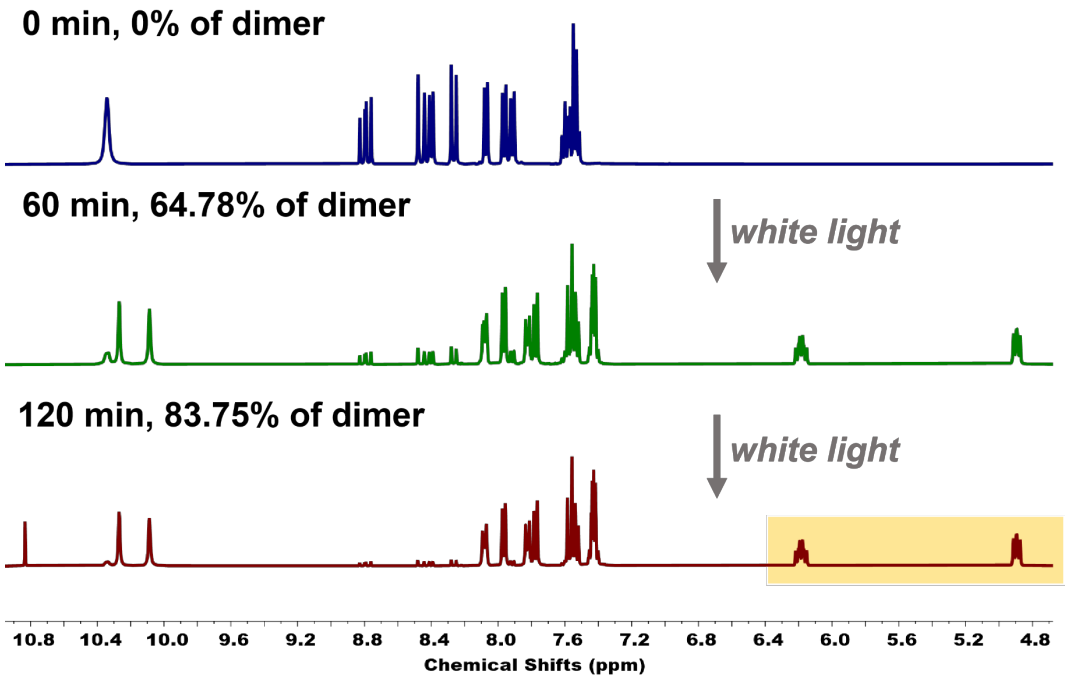

Figure S52. ^{1}H NMR spectra of Form B-W after being irradiated for different periods (THF-d_8 as the solvent).

Supplementary References:

1 T. Lu and Q. Chen, *J. Phys. Chem. A*, 2023, **127**, 7023–7035.

2 T. Lu and F. Chen, *J. Comput. Chem.*, 2012, **33**, 580–592.

3 T. Lu, *J. Chem. Phys.*, 2024, **161**, 82503.